the plant journal

SEB SOCIETY FOR EXPERIMENTAL BIOLOGY

The Plant Journal (2020) **102,** 276–298 doi: 10.1111/tpj.14623

Babo1, formerly Vop1 and Cop1/2, is no eyespot photoreceptor but a basal body protein illuminating cell division in *Volvox carteri*

Eva L. von der Heyde and Armin Hallmann*

Department of Cellular and Developmental Biology of Plants, University of Bielefeld, Universitätsstr 25, 33615 Bielefeld, Germany

Received 22 August 2019; revised 29 October 2019; accepted 19 November 2019; published online 28 November 2019.
*For correspondence (e-mail armin.hallmann@gmx.de).

SUMMARY

In photosynthetic organisms many processes are light dependent and sensing of light requires light-sensitive proteins. The supposed eyespot photoreceptor protein Babo1 (formerly Vop1) has previously been classified as an opsin due to the capacity for binding retinal. Here, we analyze Babo1 and provide evidence that it is no opsin. Due to the localization at the basal bodies, the former Vop1 and Cop1/2 proteins were renamed *V.c.* Babo1 and *C.r.* Babo1. We reveal a large family of more than 60 Babo1-related proteins from a wide range of species. The detailed subcellular localization of fluorescence-tagged Babo1 shows that it accumulates at the basal apparatus. More precisely, it is located predominantly at the basal bodies and to a lesser extent at the four strands of rootlet microtubules. We trace Babo1 during basal body separation and cell division. Dynamic structural rearrangements of Babo1 particularly occur right before the first cell division. In four-celled embryos Babo1 was exclusively found at the oldest basal bodies of the embryo and on the corresponding d-roots. The unequal distribution of Babo1 in four-celled embryos could be an integral part of a geometrical system in early embryogenesis, which establishes the anterior–posterior polarity and influences the spatial arrangement of all embryonic structures and characteristics. Due to its retinal-binding capacity, Babo1 could also be responsible for the unequal distribution of retinoids, knowing that such concentration gradients of retinoids can be essential for the correct patterning during embryogenesis of more complex organisms. Thus, our findings push the Babo1 research in another direction.

Keywords: basal bodies, basal apparatus, Volvoxrhodopsin, Chlamyrhodopsin, Vop1, Cop1/2, tubulin, *Volvox carteri, Chlamydomonas reinhardtii*, photoreceptor.

INTRODUCTION

The multicellular, spherical green microalga *Volvox carteri* (*Volvox*) serves as a model for the investigation of developmental processes including cell division, morphogenesis, and cellular differentiation (Kirk, 1998; Hallmann, 2006; Herron *et al.*, 2009; Matt and Umen, 2016). A close unicellular relative of *Volvox*, *Chlamydomonas reinhardtii*, has largely been used for studying photosynthesis, phototaxis, and light perception (Harris, 2001; Manuell and Mayfield, 2006; Harris *et al.*, 2009; Sasso *et al.*, 2018). However, if phototaxis and light perception of multicellular organisms with differentiated cells is under review, *Volvox* also is a well suited model organism (Drescher *et al.*, 2010; Ueki *et al.*, 2010; Goldstein, 2015).

Volvox shows a complete germ-soma division of labor between approximately 16 asexual reproductive cells (gonidia) and approximately 2000 somatic cells. The small somatic cells are arranged as a monolayer at the surface of a transparent sphere of extracellular matrix (ECM), whereas the large reproductive cells are embedded in the ECM just beneath the somatic cells. The mortal somatic cells are equipped with two flagella and an eyespot apparatus for light perception. These cells are thus responsible for light-regulated movement of the spheroid, whereas the potentially immortal reproductive cells represent the germline.

In *Volvox* many cellular processes are light dependent, including photosynthesis, phototaxis, sexual reproduction, circadian clock, and developmental processes such as initiation of cell division, cellular differentiation, and cell cycle control (Starr, 1980; Kirk and Kirk, 1985; Kirk, 1998; Kianianmomeni and Hallmann, 2014). To explore the molecular basis of light perception, 13 putative photoreceptor genes have been identified so far in the *Volvox* genome

(Kianianmomeni, 2015). Most of these genes show a cell-type specific expression in somatic cells that could imply a function in phototaxis and light-dependent orientation. Only one of the putative photoreceptor genes shows a cell-type specific expression in reproductive cells and it is even highly overexpressed in this cell-type (Ebnet *et al.*, 1999; Kianianmomeni, 2015; Klein *et al.*, 2017). This gene has previously been called *vop1* (Ebnet *et al.*, 1999; Kianianmomeni, 2015; Klein *et al.*, 2017) in *Volvox* and its homolog in the related algae *Chlamydomonas* was called Chlamyrhodopsin, *cop* or *cop1/2* (Deininger *et al.*, 1995; Fuhrmann *et al.*, 1999; Fuhrmann *et al.*, 2001; Greiner *et al.*, 2017). However, we now felt obliged to rename *vop1* and *cop1/2* as *babo1* because, as described below, the corresponding protein is no opsin-based photoreceptor at the eyespot but a basal body protein. From this point forward, therefore, we use only the new name '*babo1*'.

The *babo1* gene of *V. carteri* and the corresponding Babo1 amino acid sequence (formerly Vop1) (Ebnet *et al.*, 1999) have been identified through the amino acid sequence similarity between *V.c.* Babo1 and the earlier known *Chlamydomonas reinhardtii* Babo1 (formerly Cop1/2, Cre01.g002500; not to be confused with the E3 ubiquitin-protein ligase Cop1, Cre02.g085050) (Tilbrook *et al.*, 2016). Even if three splice variants have previously been predicted for *C.r. babo1* (formerly *cop1/2*), only one of these variants shows reasonable expression (Fuhrmann *et al.*, 2003) and this is also the only splice variant that is indicated in the current version of the *C. reinhardtii* genome (v5.5; gene ID Gene ID: Cre01.g002500). Therefore, we here refer to the latter variant, which corresponds to GenBank entry AF295371. The Babo1 amino acid sequences of *C. reinhardtii* and *V. carteri* share 71% sequence identity and 83% similarity. Babo1 (Cop1/2) protein of *C. reinhardtii* was initially purified from eyespot membrane preparations based on the binding of [^{3}H]retinal (Deininger *et al.*, 1995). Because only a single band appeared after gel electrophoresis of [^{3}H]retinal-labeled cell extracts and subsequent fluorography, Babo1 (Cop1/2) has been considered to be the first and only retinal-binding protein of *C. reinhardtii* (Kröger and Hegemann, 1994; Deininger *et al.*, 1995). Based on the fact that the polyene chromophore retinal is an integral component of rhodopsins and due to the much earlier result that the photoreceptor for phototaxis must be a rhodopsin (Foster *et al.*, 1984), *C.r.* Babo1 was suggested to be the rhodopsin that triggers the organism's phototactic behavior (Kröger and Hegemann, 1994; Deininger *et al.*, 1995). However, later RNAi experiments showed that *C. reinhardtii* Babo1 (Cop1/2) is definitely not the photoreceptor that is required for phototaxis (Fuhrmann *et al.*, 2001) and soon afterwards two retinal-binding channelrhodopsins were identified in *C. reinhardtii* (Nagel *et al.*, 2002; Sineshchekov *et al.*, 2002; Nagel *et al.*, 2003; Suzuki *et al.*, 2003), which actually mediate photomovement responses (Sineshchekov *et al.*, 2002).

Once it was clear that Babo1 cannot be the photoreceptor for phototaxis, the intriguing question arose what was the real function of this protein. It also requires clarification that Babo1 proteins of *C. reinhardtii* and *V. carteri* were postulated to have, at most, four hydrophobic membrane-spanning segments (Deininger *et al.*, 1995; Ebnet *et al.*, 1999), even though all known rhodopsins have at least seven transmembrane helices (Gao *et al.*, 2015). Our attention was also attracted by the fact that we were not able to detect any convincing sequence similarity between Babo1 proteins and experimentally confirmed photoreceptor domains. Another peculiarity of Babo1 is its cell-type specific expression: *babo1* mRNA was shown to be approximately 10-fold overexpressed in reproductive cells when compared with somatic cells (Kianianmomeni and Hallmann, 2015) and a similar cell-type specific distribution has been shown for the Babo1 protein (Ebnet *et al.*, 1999). This distribution is remarkable because both a whole transcriptome RNA-seq analysis of separated cell types (Klein *et al.*, 2017) and a cell-type specific expression analysis of selected genes (Kianianmomeni and Hallmann, 2015) showed that the known photoreceptor genes of *Volvox* are predominantly expressed in somatic cells (or in rare cases show no cell-type-specific expression), whereas *babo1* is the only (putative) photoreceptor gene that is overexpressed in reproductive cells.

In addition to these conspicuous features, the previous information about the localization of Babo1 within the cell is ambiguous. Initially, *C.r.* Babo1 was purified from eyespot membrane preparations (Deininger *et al.*, 1995) and assigned with an eyespot localization also due to immunolocalization experiments (Deininger *et al.*, 1995), GFP-tagging (Fuhrmann *et al.*, 1999) and due to its identification within the eyespot proteome (Schmidt *et al.*, 2006; Wagner *et al.*, 2008). However, *V.c. babo1* shows only weak expression in the eyespot-containing somatic cells of *Volvox*, whereas the reproductive cells, which actually have no eyespot at all, show strong expression of *babo1* (Kianianmomeni and Hallmann, 2015). The situation becomes even more confusing by the fact that *C.r.* Babo1 was also identified in thylakoid-enriched fractions (Allmer *et al.*, 2006) and was suggested to be part of the Ycf4-photosystem I assembly complex (Ozawa *et al.*, 2009). It also was proposed that Babo1 is a sensory light receptor, which influences biosynthesis of chloroplast-related proteins and photosynthetic activity in a light-dependent manner (Kianianmomeni and Hallmann, 2014).

So far, no rigorous *in vivo* localization study of Babo1 has been performed and the previously suggested localizations of Babo1 mainly resulted from indirect observations that even contradicted each other.

In this study, we analyze the sequence of Babo1 (Vop1, Cop1/2) and provide evidence that Babo1 is no transmembrane protein and, thus, cannot be an opsin. We also reveal a large family of more than 60 Babo1-related proteins from a wide range of green algae species (Chlorophyta) and we perform a molecular phylogenetic analysis. Sequence alignments not only allow for a reassessment of the conservation of critical amino acid residues, but also for clarification of the previously supposed similarity to regular rhodopsins and retinal-binding pockets. Moreover, the detailed subcellular localization of fluorescence-tagged Babo1 protein is analyzed *in vivo* using confocal laser-scanning microscopy (CLSM). We show that Babo1 is neither localized in the chloroplast nor in the eyespot of *V. carteri*. Instead, Babo1 clearly accumulates at the basal apparatus of both somatic and reproductive cells. The former names Vop1 (Volvoxopsin, Volvoxrhodopsin1) and Cop1/2 (Chlamyopsin1/2, Chlamyrhodopsin1/2) therefore turned out to be unsuitable and the proteins, therefore, were renamed *V.c.* Babo1 and *C.r.* Babo1 due to their localization at the basal bodies. The localization at the basal apparatus also verifies that Babo1 is no membrane protein and that it is not even associated with membrane structures. Eventually, we were able to trace fluorescence-tagged Babo1 protein together with the basal apparatus during basal body separation and cell division. Overall, we can clarify previous contradictions regarding the structure and localization Babo1 and we provide implications for its function.

RESULTS

Gene and mRNA sequences of *babo1*

The mRNA and genomic sequences of *babo1* of *V. carteri* (formerly *vop1*) were investigated for the first time in 1999 by the group of Peter Hegemann (Ebnet *et al.*, 1999) (GenBank entries Z69301 and Y11204). However, our *babo1* sequencing results slightly deviate from these previous results, but they coincide with the corresponding sequences of the *V. carteri* genome project (v.2.1, Vocar.0024s0227) (Prochnik *et al.*, 2010) in Phytozome 12 (Goodstein *et al.*, 2012). The differences are highlighted in Figure S1. The *babo1* gene is located on scaffold 24, the start codon is at nucleotide position 1733480 on the reverse strand, and its genomic size is approximately 3.1 kb including UTRs and promoter region. The predicted total length of the *babo1* mRNA is 1689 bp, which is slightly larger than stated earlier (1566 bp, accession number Z69301, (Ebnet *et al.*, 1999)). An alignment of RNA sequencing data (Klein *et al.*, 2017) and EST data (Prochnik *et al.*, 2010) to the *babo1* gene revealed that the 5′UTR of *babo1* has a length of 48 bp, which was predicted correctly in the *V. carteri* genome data of Phytozome 12, while the 5′UTR is shorter in Ebnet *et al.*, 1999. The 3′UTR, however, is approximately 100 bp shorter than predicted by the *V. carteri* genome annotation, but corresponds instead to the 3′UTR presented by Ebnet *et al.* (1999). The comparison of mRNA and genomic sequences shows that the *babo1* gene contains seven introns with sizes from 69 to 375 bp. The number of seven introns corresponds to the average number of introns per gene in the *V. carteri* genome (v.2.1), which is precisely 7.05 (Prochnik *et al.*, 2010). However, the sizes of the *babo1* introns are all below the average intron length of all introns in all nuclear genes, which is 399.5 bp (Hanschen *et al.*, 2016). The below-average intron sizes might be relevant, because genes with basic cellular activity (housekeeping genes) frequently have shorter introns (Eisenberg and Levanon, 2003; Carmel and Koonin, 2009; Eisenberg and Levanon, 2013).

Sequence analysis of Babo1

The 735-bp coding sequence of the *babo1* mRNA encodes a polypeptide of 244 amino acids with an expected molecular mass of 26.4 kDa. Babo1 thus belongs to the smaller proteins of *V. carteri*. The comparison of the amino acid composition of Babo1 with the amino acid composition of the *V. carteri* (v.2.1) proteome (Prochnik *et al.*, 2010), which was deduced from all *V. carteri* genes in Phytozome 12 (Goodstein *et al.*, 2012), revealed that the basic amino acid lysine is found much more frequently in Babo1 than in the average of all *V. carteri* proteins (Figure S2). The lysine content of Babo1 is 17.2%, which corresponds to every sixth amino acid of Babo1 and 42 lysine residues in total, whereas the average lysine content of all proteins is just 3.5% (Figures 1 and S2). In addition to lysine, there are two other amino acids with side chains that can be positively charged in aqueous solution (at neutral pH): arginine and histidine. However, the percentage share of the two latter amino acids appears to be below average in Babo1, rather than increased (Figure 1).

Previously, Babo1 (formerly Vop1) was identified as a 30 kDa protein in membrane fractions of *V. carteri* and, mainly based on sequence similarities, its presence in membrane fractions and due to results with antisense transformants, it was believed to be a membrane receptor of an algal opsin family (Ebnet *et al.*, 1999). Due to inconsistencies that arose from our preliminary CLSM experiments that localized Babo1 away from any membrane structures and the fact that opsins or other membrane receptors are necessarily embedded in a membrane, we reinvestigated the Babo1 amino acid sequence with regard to transmembrane spanning segments. We used bioinformatics tools that searched for similarities between Babo1 and verified transmembrane proteins, utilized algorithms that were trained on transmembrane protein datasets, and also analyzed Babo1 only based on its sequence of amino acid residues. The battery of applied programs included

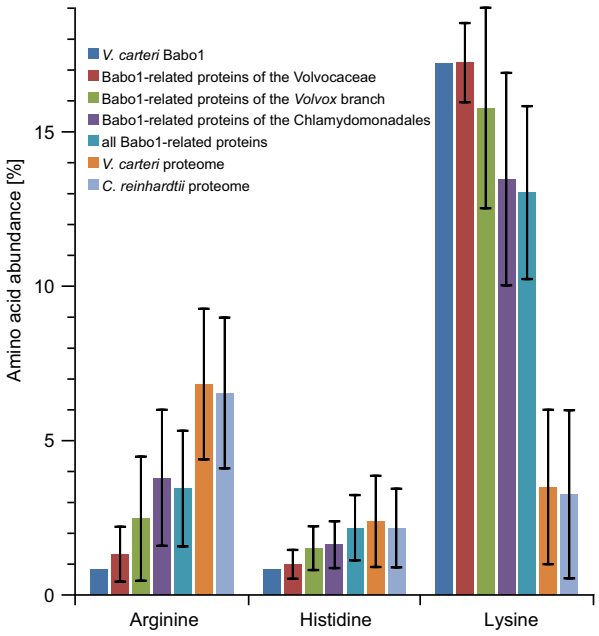

Figure 1. Relative abundance of basic amino acids in Babo1, Babo1-related protein groups, and the proteomes of *Volvox carteri* and *Chlamydomonas reinhardtii*. The relative abundance of basic amino acids was calculated for *V. carteri* Babo1, all Babo1-related proteins shown in Figure 2, for subgroups within Figure 2, and for proteomes of *V. carteri* and *C. reinhardtii*. The subgroups are as follows: the Babo1-related proteins of the Volvocaceae family, the Babo1-related proteins of the *Volvox* branch and the Babo1-related proteins of the Chlamydomonadales order. The Babo1-related proteins are listed in Table S4. Error bars represent the standard deviation. The relative abundance data for all 20 canonical amino acids are shown in Figure S2.

TMSEG (Bernhofer *et al.*, 2016), PolyPhobius (Käll *et al.*, 2005; Käll *et al.*, 2007), Phobius (Käll *et al.*, 2004; Käll *et al.*, 2007), MEMSAT3 (Jones *et al.*, 1994), MEMSAT-SVM (Nugent and Jones, 2009), PHDhtm (Rost *et al.*, 1995; Combet *et al.*, 2000), TMHMM (Krogh *et al.*, 2001), TMpred (Hofmann and Stoffel, 1993), DAS-TMfilter (Cserzo *et al.*, 2004), MINNOU (Cao *et al.*, 2006), TBBpred (Natt *et al.*, 2004), PRED-TMR2 (Pasquier and Hamodrakas, 1999), and the Kyte and Doolittle hydrophobicity plot (Kyte and Doolittle, 1982). However, no transmembrane spanning segments have been identified and all of these programs predicted that Babo1 is not a transmembrane protein. Moreover, when yellow fluorescent protein (YFP)-tagged Babo1 of *C. reinhardtii* (formerly Cop1/2) was expressed in *Xenopus* oocytes, YFP fluorescence was exclusively found in the soluble fraction of oocyte extracts but not in the membrane fraction (Tian *et al.*, 2018). As a consequence of these results, Babo1 cannot be an opsin, which would necessarily require a transmembrane structure with generally seven transmembrane helices. Thus, the former name 'Vop1', which stood for Volvoxopsin 1, was no longer justified and we renamed the protein Babo1.

Identification of a large family of Babo1-related proteins

Babo1 of *V. carteri* (formerly Vop1) has previously been identified due to is similarity with Babo1 of *C. reinhardtii* (formerly Cop1/2) (Deininger *et al.*, 1995; Ebnet *et al.*, 1999). These homologous proteins show 71% identity and 83% similarity. The coding sequences of the corresponding genes show 77% identity and the number and even position of the seven introns is conserved between the two *babo1* sequences. Due to this significant evolutionary conservation between *Volvox* and *Chlamydomonas*, we searched for further Babo1-related proteins in other species using transcriptome data of the 1000 plants project (1KP) (Matasci *et al.*, 2014) and the database resources of the National Center for Biotechnology Information (NCBI Resource Coordinators, 2018). Identified sequences that were too short, had gaps, had low similarity values, or that showed any other types of ambiguity were excluded from further analysis. Despite this strict quality control, we identified previously unknown Babo1-related proteins in more than 60 species. All Babo1-related proteins were identified in green algae or, more precisely, within the core chlorophytes (Turmel *et al.*, 2009). The identified Babo1-related proteins originated from morphologically and ecologically divers chlorophytes, which included (i) unicellular and multicellular genera (e.g. *Chloromonas* in Chlamydomonadales and *Codium* in Ulvophyceae); (ii) microalgae and macroalgae (e.g. *Hafniomonas* in Chlamydomonadales and *Acrosiphonia* in Ulvophyceae); (iii) freshwater, marine and saline algae (e.g. *Eudorina* in Volvocaceae, *Halochlorococcum* in Ulvophyceae and *Dunaliella* in Chlamydomonadales); and (iv) algae having cells with no, two, or even four flagella (e.g. *Chlorella* in Chlorellales, *Gonium* in Volvocaceae, and *Tetraselmis* in Chlorodendrophyceae). A multiple alignment of all Babo1-related proteins used in this study is shown in Figure S3. The alignment shows that the greatest degree of conservation among the Babo1-related proteins is found between amino acid positions 108 to 129 of the alignment in Figure S3. The amino acids Q_{80}, P_{83}, P_{91}, and P_{93} of *V.c.* Babo1 showed the highest degree of conservation among all Babo1-related proteins. However, these amino acids are not conserved in vertebrate opsins and the corresponding part of the sequence previously was not thought to be particularly significant (Deininger *et al.*, 1995; Ebnet *et al.*, 1999); instead it was considered that K_{228} in the motif $AKA_{227\text{-}229}$ close to the C-terminus of *V. carteri* Babo1 is a conserved retinal binding lysine (Ebnet *et al.*, 1999). Figure S3 clearly shows that K_{228} is not conserved and the sequence area immediately around K_{228}, which previously has been called retinal binding site or retinal-binding region (Ebnet *et al.*, 1999), is the area with the lowest degree of similarity among all 64 Babo1-related proteins. Furthermore, for Babo1 of *C. reinhardtii* (formerly Cop1/2), C_{21} and C_{115} were suggested to

form an intramolecular disulfide bridge (Deininger *et al.*, 1995). Not only does the alignment show that there are no conserved cysteines at these positions or elsewhere, but even half of the Babo1-related proteins have less than two cysteines in their entire amino acid sequence. Therefore it is impossible that these proteins form intramolecular disulfide bridges.

To reveal evolutionary relationships within the family of Babo1-related proteins, we performed a molecular phylogenetic analysis. The generated unrooted bootstrap consensus tree of Babo1 and 63 Babo1-related proteins is shown in Figure 2. In this tree, *V. carteri* Babo1 (Volcar857) branches within the Volvocaceae family, as expected. Babo1 of *C. reinhardtii* branches close to the Volvocaceae family within the Chlamydomonadales order. Other Babo1-related proteins build subgroups that are consistent with the evolutionary relationship of the corresponding organisms. The bootstrap values within quite a few subgroups show a good support (>70%). However, several of the deep branches are uncertain due to low bootstrap values. As an example, previous molecular phylogenetic analyses indicate that the Chlamydomonadales are somewhat more closely related to the Ulvophyceae than to the Chlorellales within Trebouxiophyceae (Leliaert *et al.*, 2012) but our molecular phylogenetic analysis can neither support nor oppose this assumption.

In consideration of our BLAST search results and the molecular phylogenetic analysis, there is no evidence of lateral gene transfer or convergent evolution of Babo1-related genes. There is also no indication of gene loss in any of the subgroups of the core chlorophytes even if we excluded some Babo1-related sequences (and thus species) due to our strict quality rules. We identified however *babo1* gene duplicates in the genomes of some analyzed species (marked in Figure 2). The distribution of species with *babo1* gene duplicates is scattered among the analyzed core chlorophytes. Moreover, the gene copies within an affected genome are identical or almost identical to each other. Both observations suggest recent and independent *babo1*-duplication events.

Amino acid composition of Babo1-related proteins

The noticeably high lysine content of *V. carteri* Babo1 (17.2%) prompted us to investigate the amino acid composition of all Babo1-related proteins (Figures 1 and S2). The lysine content of both the Babo1-related proteins of the Volvocaceae family and of the whole *Volvox* branch within the Chlamydomonadales is approximately as high as in *V. carteri* Babo1 (Figures 1 and S2). Similarly, when looking at the Babo1-related proteins of the entire Chlamydomonadales order or even at all investigated Babo1-related proteins, the average lysine content is not less than 13%. By contrast, the average lysine content of all proteins both in the *V. carteri* proteome and the *C. reinhardtii* proteome is less than 4% (Figures 1 and S2). Although the high lysine content is well conserved among Babo1-related proteins, the exact amino acid position of most of the lysines seems to be less important because the lysine residues do not stand out from the multiple alignment (Figure S3).

For a better assessment of the high lysine content of Babo1-related proteins, we sorted all proteins of both the *V. carteri* or *C. reinhardtii* proteomes by their lysine content. *V. carteri* Babo1 ranks 36th and *C. reinhardtii* Babo1 ranks 65th among more than 14 000 predicted proteins each. As expected, there are predominantly histones and ribosomal proteins among the most lysine-rich proteins (Tables S1 and S2) because positively charged lysines bind nucleic acids by interacting with the negatively charged phosphate moiety in their backbone. Apart from the charge-mediated binding potential, the ε-amino groups of lysine residues allow for post-translational modifications. In fact, lysine is essentially the most highly post-translationally modified amino acid out of the 20 naturally encoded amino acids (Zee and Garcia, 2012).

Production of *Volvox* transformants expressing fluorescence-tagged Babo1 and β2-tubulin

With regard to a rigorous *in vivo* localization of Babo1, *Volvox* is much more suitable than *Chlamydomonas* because the reproductive cells of *Volvox* exceed the volume of *Chlamydomonas* cells by more than 100 times, which significantly facilitates the accurate localization. To visualize the expression of Babo1 in living cells of *Volvox*, a chimeric gene was constructed that allows for expression of a fusion protein in which the *C*-terminus of *V.c.* Babo1 is fused via a pentaglycine interpeptide bridge (Gly5) to a YFP (Figure 3a). The chimeric gene is driven by the endogenous *V.c. babo1* promoter region and terminated by the endogenous *V.c. babo1* terminator region (Figure 3a). This construction allows for a *babo1/yfp* expression level that is comparable with the *babo1* expression level under natural conditions. In a similar DNA construct, *babo1/yfp* is driven by the constitutive and strong *LHCBM1* promoter region (Figure 3b). For *in vivo* co-localization of Babo1 and microtubules, another chimeric gene was constructed that allows for expression of a fusion protein in which the N-terminus of β2-tubulin is fused to a cyan fluorescent protein (CFP) (Figure 3c). The chimeric gene is driven by the endogenous *tubB2* promoter region. In a similar DNA construct, *cfp*/*tubB2* was brought under the control of the constitutive and strong *LHCBM1* promoter region (Figure 3d).

For stable nuclear transformation of *V. carteri* strain TNit-1013, three vectors were used simultaneously: babo1 fused to the *yfp* reporter gene (Figure 3a), the *cfp* reporter gene fused to *tubB2* (Figure 3c) and pVcNR15 as a selectable marker. The obtained transformants were investigated

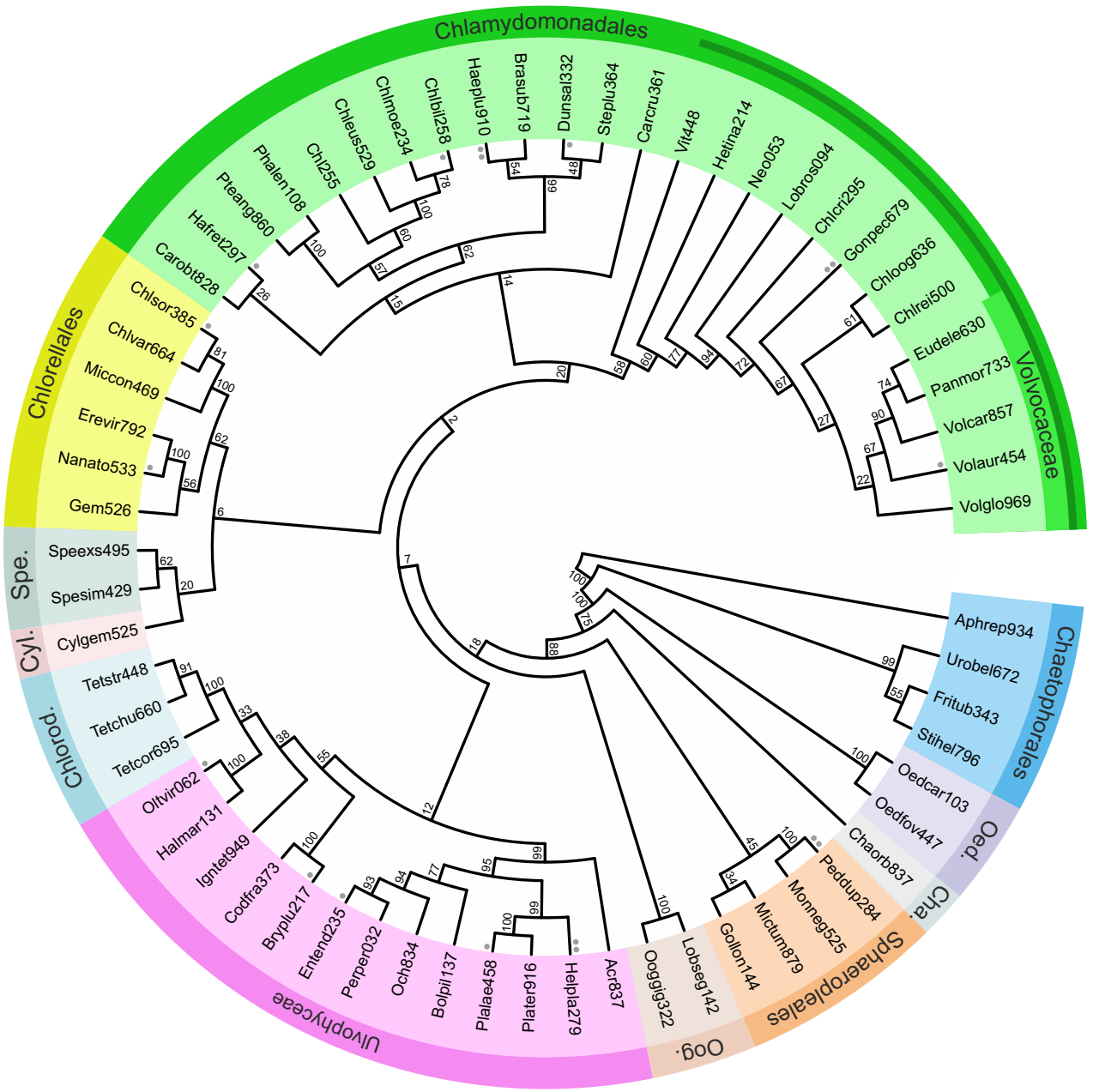

Figure 2. Phylogenetic tree of Babo1-related proteins. Sequence relationship between *Volvox carteri* Babo1 (Volcar857) and 63 Babo1-related proteins from green algae (Chlorophyta), as listed in Table S4. The unrooted bootstrap consensus tree is based on 10 000 replicates calculated using the neighbor-joining method (Saitou and Nei, 1987). The bootstrap values of the branch points are indicated. Babo1 of *V. carteri* (Volcar857) can be found in the Volvocaceae subgroup, which is part of the *Volvox* branch (dark green circular arc) of the Chlamydomonadales. In most species, *babo1* is a single-copy gene, however, in some species there are one (●) or two (●●) additional, almost identical gene copies in the genome. Cha., Chaetopeltidales; Chlorod., Chlorodendrophyceae; Cyl., Cylindrocapsa-clade of Sphaeropleales (Müller *et al.*, 2004); Oed., Oedogoniales; Oog., Oogamochlamys-clade in Chlorophyceae (Pröschold *et al.*, 2001); Spe., Spermatozopsis lineage (Lemieux *et al.*, 2015).

for stable genomic integration of the DNA constructs and expression of the desired proteins at sufficient levels, which was examined by fluorescence microscope-based screening. Twenty-nine percent of the transformants expressed only the nitrate reductase but showed no fluorescence. Fifty-nine percent only showed YFP fluorescence, which originates from the Babo1–YFP fusion protein. The remaining 14% of the transformants expressed all three plasmids to sufficient extent. The transformant strains were synchronized by a light–dark cycle and the integrity of cell division and embryogenesis was microscopically verified.

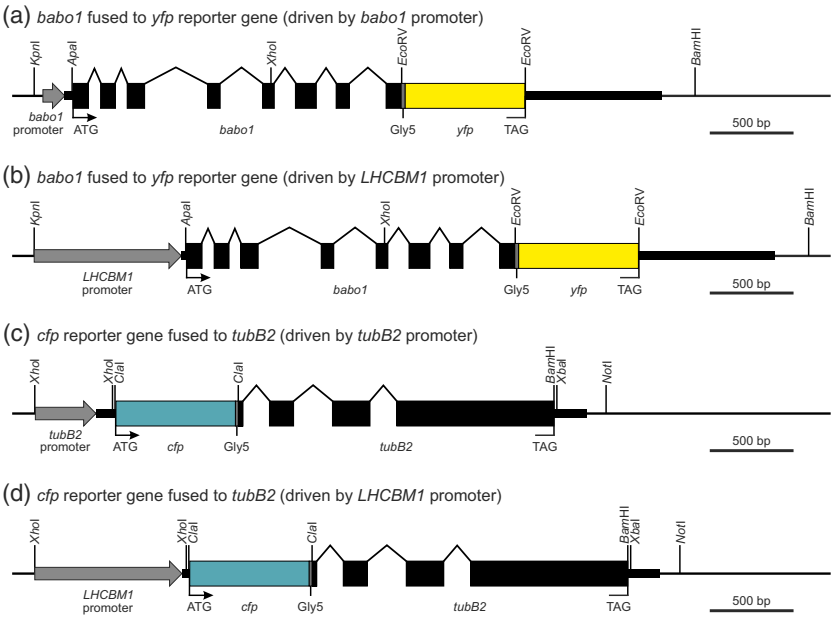

Figure 3. Vectors for expression of *babo1* and *tubB2* genes fused to fluorescent reporter genes. (a) The *Volvox carteri babo1* gene that contains seven endogenous introns was fused to the *yfp* reporter gene; the chimeric gene is driven by the *V. carteri babo1* promoter region (gray arrow). (b) The *V. carteri babo1* gene was fused to the *yfp* reporter gene; the chimeric gene is driven by the *V. carteri LHCBM1* promoter region (gray arrow). (c) The *cfp* reporter gene was fused to the *V. carteri tubB2* gene; the chimeric gene is driven by the *V. carteri tubB2* promoter region (gray arrow). (d) The *cfp* reporter gene was fused to the *V. carteri tubB2* gene; the chimeric gene is driven by the *V. carteri LHCBM1* promoter region (gray arrow). (a–d) A short linker sequence, which codes for a flexible pentaglycine interpeptide bridge (Gly5), was inserted between each gene of interest and reporter gene. The 5′ and 3′ untranslated regions are represented by thick black lines and angled lines depict introns. The positions of start (ATG) and stop (TAG) codons and of restriction sites used for cloning are indicated. The pBluescriptII SK(−) vector backbones are not shown.

Babo1 is not located at the eyespot

Previously, Babo1 was classified as an opsin and it was thought to be localized at the eyespot (Deininger *et al.*, 1995; Ebnet *et al.*, 1999; Fuhrmann *et al.*, 1999). However, when transformed algae expressing Babo1–YFP (and TubB2-CFP) were excited with 514 nm light, the corresponding YFP signal appeared at the flagellar bases of somatic cells (Figure 4a,b,d). Such a signal did not occur in wild-type control cells (Figure 4g,h,j). In the eyespots of both transformants and wild-type control cells, only an autofluorescence signal was detectable (Figure 4b,h), which was much weaker than the YFP signal at the flagellar bases and, therefore, it was only visible under overexposure conditions. Excitation at 405 nm stimulated the TubB2–CFP fluorescence, which shows the cytoplasmic microtubules at the flagellar base and the axonemal microtubules of the flagella of somatic cells (Figure 4c,d). The chlorophyll fluorescence shows the position of the single, large chloroplast with its meshwork-like structure (Figure 4e,k).

In order to unequivocally distinguish YFP fluorescence from autofluorescence, lambda scans were performed that allow the separation of spatially overlapping emission signals. More precisely, mean fluorescence spectra for selected subcellular regions of somatic cells were measured and compared both with each other and with the YFP spectrum. This procedure allowed for an unambiguous assignment of emission signals to the corresponding fluorescent molecules. After excitation at 514 nm, the fluorescence emitted from the basal bodies peaked at approximately 530 nm and reached about 1700 rlu (Figure 5a). Both the peak position and the shape of the spectrum is typical for the utilized YFP variant (Kremers *et al.*, 2006). By contrast, the fluorescence emitted from the eyespot had its maximum at about 557 nm and it reached only about 235 rlu. Moreover, the eyespot fluorescence spectrum of Babo1–YFP transformants was identical to the eyespot fluorescence spectrum of untransformed wild-type cells (Figure 5b). A pictorial representation of these data was generated by spectral imaging, also known as lambda view. Under this method, a color palette, mimicking the emission wavelength of the channel, is automatically assigned to the individual lambda images which are then displayed in a merge-type display. In lambda view, the flagellar bases appeared in blue-green color (Figure 5d), whereas the eyespot fluorescence was clearly characterized by longer wavelengths and thus appeared as a yellow-green color (Figure 5e). Thus, our results clearly demonstrated that only the basal bodies of transformants emitted the expected YFP spectrum of Babo1–YFP, whereas eyespots exclusively exhibit weak autofluorescence. Because

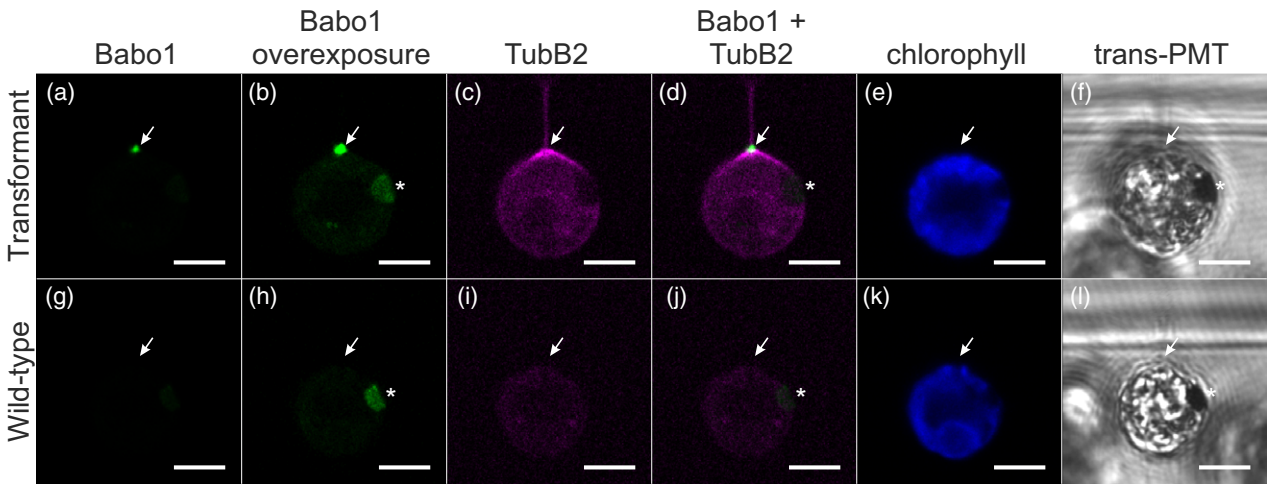

Figure 4. CLSM images of a Babo1–YFP/TubB2–CFP co-transformant and of the wild-type. (a–f) Side view of a somatic cell of a *Volvox carteri* co-transformant expressing both Babo1–YFP and TubB2-CFP. (g–l) Side view of a somatic cell of the untreated *V. carteri* wild-type. (a, b, d, g, h, j) For YFP localization, excitation was at 514 nm and detection was at 517–553 nm (green). (c, d, i, j) For CFP localization, excitation was at 405 nm and detection was at 460–500 nm (magenta). (e, k) For chlorophyll localization, excitation was at 405 nm and detection was at 651–700 nm (blue). (a–e and g–k) *In vivo* CLSM images. (f, l) *In vivo* images detected by transmitted light photomultiplier tube (*trans*-PMT). (a–l) The positions of the basal bodies (arrow) and the eyespot (asterisk) are indicated. Scale bars = 5 μm.

basal bodies of wild-type cells showed no autofluorescence at all, the total amount of detected basal body fluorescence of transformants can be assigned to Babo1–YFP.

Overexpression of Babo1 negatively affects the viability of transformants

One of our further objectives was to investigate the effects of an increased expression of Babo1. For this purpose, transformation of *V. carteri* was performed using a plasmid that drives the expression of Babo1–YFP with the constitutive and strong *LHCBM1* promoter region (Figure 3b) instead of the endogenous *babo1* promoter region used before (Figure 3a). However, with this modified approach we were not able to generate any transformants and this indicated that strong overexpression of Babo1 negatively affects the viability of transformants. Likewise, we obtained no transformants when we highly overexpressed the fluorescence-tagged TubB2 under the control of the *LHCBM1* promoter region (Figure 3d).

These results are in accordance with previous reports where overexpression of GFPα2-tubulin in *S. pombe* was lethal, whereas moderate expression had no negative effects (Ding *et al.*, 1998). In the green alga *C. reinhardtii*, the attempt to express GFP fusions of 10 different basal body and flagella proteins was almost without success: only one construct resulted in viable transformants that showed successful expression of the desired fusion protein (Schoppmeier *et al.*, 2005). Therefore, overexpression of basal body and cytoskeletal components may have a negative impact on cell division and, thus, also on the viability and survival rate of transformants.

High-resolution localization of Babo1 at the basal apparatus

The two distinct cell types of *V. carteri* significantly differ in structure and function (Kirk, 1998) (Figure 6d). In transformants expressing Babo1–YFP under the control of the *babo1* promoter region (Figure 3a), Babo1 can be found in both cell types, the small biflagellated somatic cells and the large flagella-less reproductive cells (gonidia). Because we utilized the original, endogenous promoter region, it reflects the natural expression pattern of Babo1. Figure 6(a,b) shows young daughter spheroids of transformed algae expressing Babo1–YFP. When viewed from outside onto the surface of the spheroid, each somatic cell exhibits two distinct fluorescent dots at the center of the cells just below the plasma membrane that correspond to Babo1–YFP at the two basal bodies (Figure 6a). The basal bodies of neighboring cells show the same orientation, which is a fundamental precondition for ensuring that the flagella beat into the same direction and that the whole spheroid swims in one specific direction. Even though the reproductive cells are flagella-less, they still have basal bodies. Consequently, each reproductive cell exhibits two fluorescent dots, which correspond to the Babo1–YFP at the basal bodies (Figure 6b). The basal bodies appear brighter in the large reproductive cells than in the small somatic cells and, therefore, seem to contain more Babo1–YFP protein. The highest fluorescence intensity is detected in the center of each basal body, which might indicate, that Babo1 is located in the lumen of the basal bodies.

Even if most of the Babo1–YFP fluorescence co-localizes with the basal bodies, a smaller proportion of the

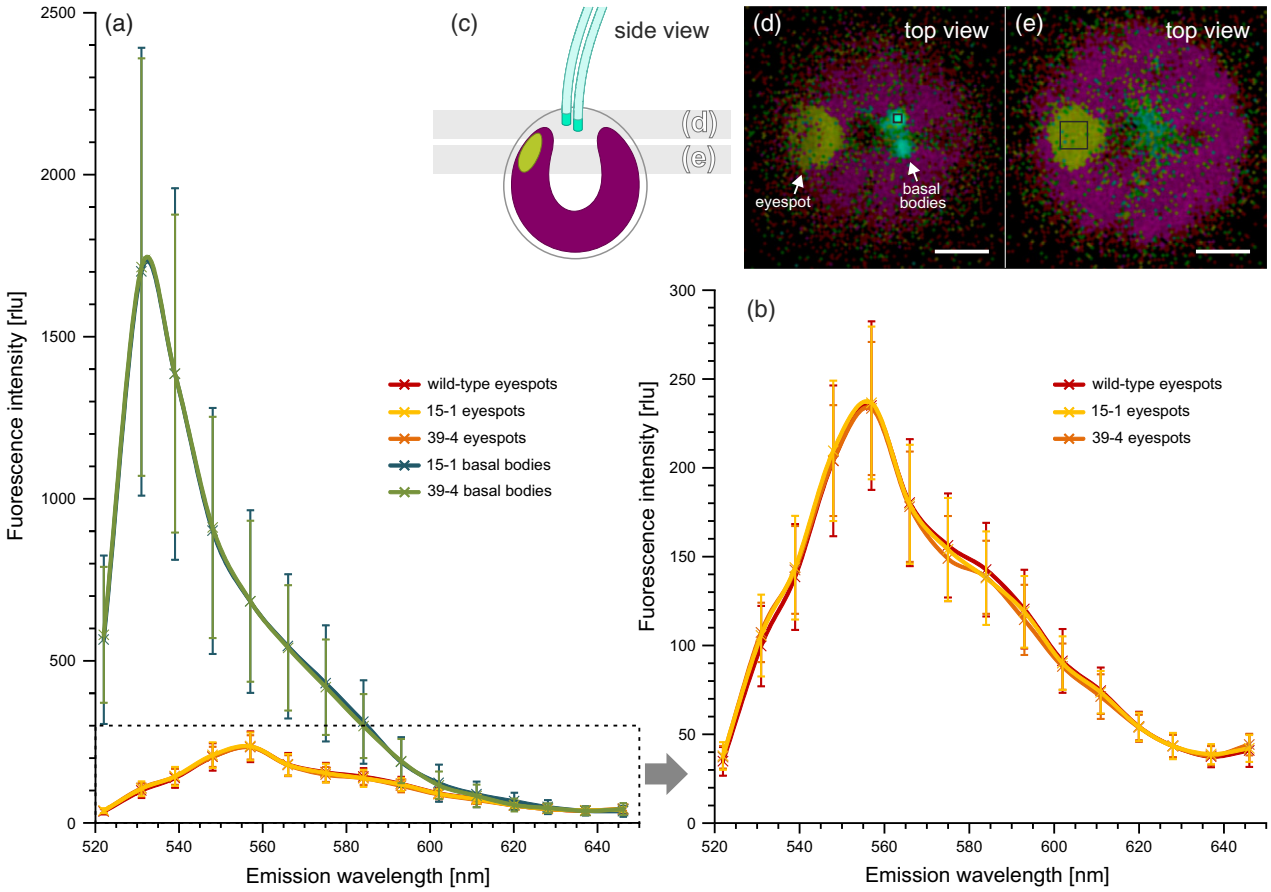

Figure 5. Fluorescence spectra of basal bodies and eyespots of Babo1–YFP transformants compared with the wild-type. (a) Fluorescence spectra (lambda scans) of basal bodies and eyespots were recorded *in vivo* in somatic cells of two independent Babo1–YFP transformants (15-1 and 39-4) and the wild-type. The fluorescence intensity was determined simultaneously in 15 different channels during excitation at 514 nm. Mean fluorescence intensities were plotted against the mean emission wavelength for each channel. Error bars represent the standard deviation ($n \geq 25$ cells per sample). Because basal bodies of wild-type cells show no fluorescence when excited at 514 nm, both adjustment of the focal plane for the measurement and selection of an adequate region of interest for lambda scanning is impossible in the wild-type. (b) Enlarged view of the framed section of (a) showing the fluorescence spectra of eyespots. (c) Schematic side view of a somatic cell showing the positions of the imaged focal planes. (d, e) Spectral imaging: *in vivo* CLSM scans operated in lambda mode showing a somatic cell of a Babo1–YFP transformant. The viewing direction is from outside of the *Volvox* spheroid onto the flagellar end of the somatic cell. The positions of the focal planes are shown in (c). Regions of interest (ROIs; black squares) within the basal bodies and eyespots were manually selected for measurement of the fluorescence spectra. The displayed colors are equivalent to the actual fluorescence wavelengths. Scale bars = 2 μm.

fluorescence can be found in the surrounding area of the basal bodies. Because reproductive cells are considerably larger than somatic cells, fine structures are much easier to observe in reproductive cells. In these larger cells, straight strands of fluorescent material were visible that lead outwards from a center at the basal bodies. The location of these strands matches the expected position of the four microtubular rootlets (Figure 6b,f). At this point in development, an unambiguous detection of microtubules was not possible, because the TubB2-CFP signal was too weak. However, later in development, shortly before embryogenesis, a more compact arrangement of microtubules arose that could be visualized by detection of TubB2–CFP. This also allowed for disclosure of the microtubule organizing center (MTOC) with its microtubules emerging close to the basal bodies (Figure 6c). The MTOC and the basal bodies are localized just beneath the surface of the mature reproductive cell. A light microscopic image of *V. carteri* in Figure 6(d) illustrates the arrangement of cells and a schematic cross-section of part of a spheroid in Figure 6(e) indicates the viewing direction for easier orientation. A schematic representation of the basal apparatus of *V. carteri* is shown in Figure 6(f). Each basal body is attached to two microtubular rootlets (MTRs): the two-membered d-root and the four-membered s-root (Moestrup, 1978). Striated microtubule-associated fibers (SMAFs) overlay the proximal part of the four microtubular rootlets (Geimer and Melkonian, 2004). The distribution of SMAFs at the microtubular rootlets correlates with that of Babo1–YFP. This becomes even clearer at the stage immediately before the two basal bodies separate from each other (to be described later). The strongest signal of Babo1–YFP was

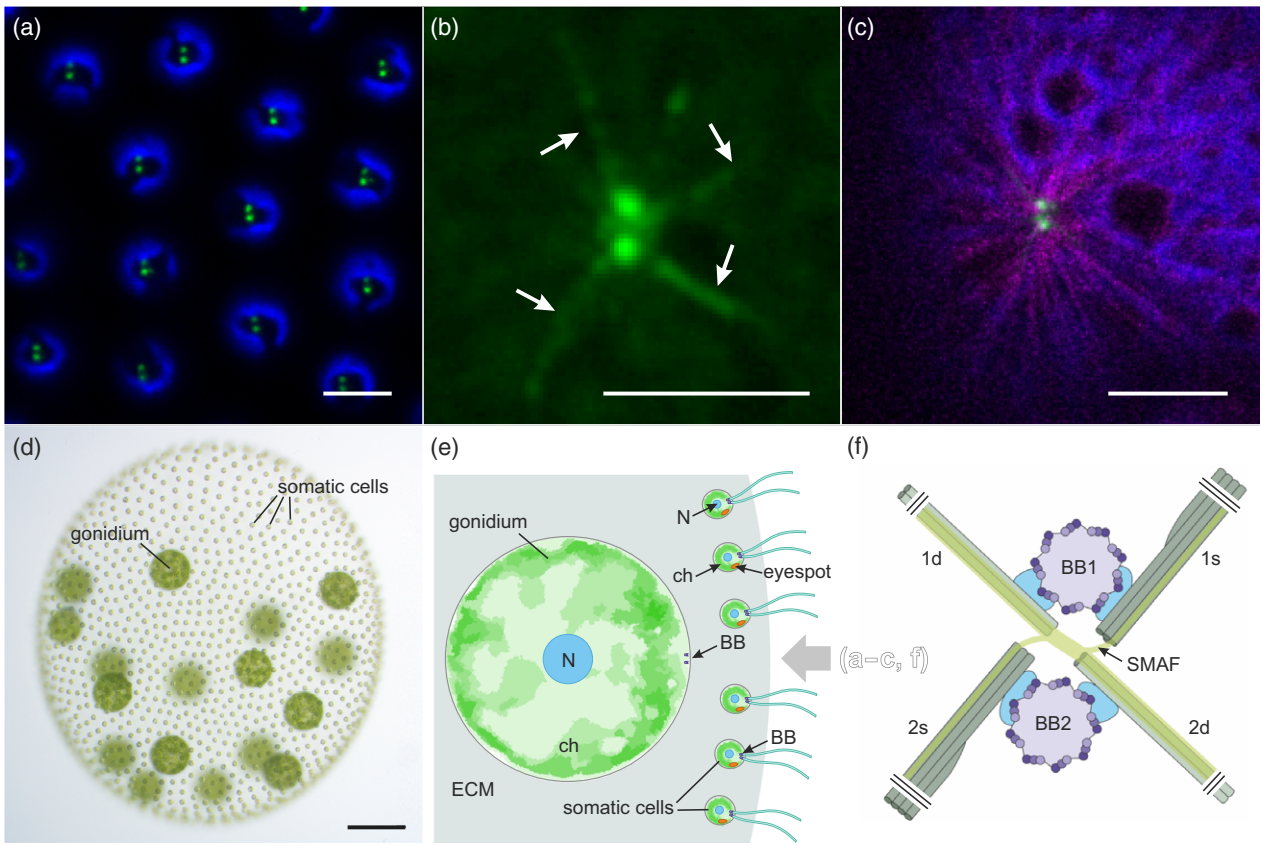

Figure 6. *In vivo* localization of Babo1–YFP in somatic cells and gonidia of *Volvox carteri*. (a) Somatic cell layer. Co-localization of Babo1–YFP (green) and chlorophyll (blue). The two punctiform Babo1–YFP signals within each cell are located immediately beneath the plasma membrane at the position of the two basal bodies. Note the regular arrangement of the basal body pairs in all cells. (b) Immature gonidium expressing Babo1–YFP (green). The two, bright circular, filled areas with the strongest fluorescence in the center indicate Babo1–YFP localization at the basal bodies. Babo1–YFP also localizes to the position of the striated microtubule-associated fibers (SMAFs), which overlay the microtubular rootlets (arrows). (c) Mature gonidium (about 24 h older than the gonidium in (b)). Co-localization of Babo1–YFP (green), TubB2–CFP (magenta) and chlorophyll (blue). At this developmental stage, microtubule fibers originating from the microtubule-organizing center (MTOC) at the basal body root complex are clearly visible. (a–c) CLSM images. The viewing direction is from outside onto the surface of the spheroid. Scale bars = 5 μm. (d) Light microscopic image of *V. carteri* illustrating the arrangement of cells. Scale bar = 100 μm. (e) Schematic cross-section of part of a *V. carteri* spheroid. A gray arrow indicates the viewing direction in (a–c) and (f). BB, basal body; ch, chloroplast; N, nucleus; ECM, extracellular matrix. (f) Schematic representation of the basal apparatus (Kirk, 1998; Geimer and Melkonian, 2004; Geimer and Melkonian, 2005). Each basal body (BB) consists of nine triplet microtubules that constitute the walls of a hollow cylinder. Basal bodies are connected both with a two-membered MTR (d-root, d for dexter) and a four-membered MTR (s-root, s for sinister) via a set of different fibers (light blue). Note that the proximal end of one s-root microtubule is located below the other three. SMAFs (yellow green) are overlaying only the proximal part of the MTRs, which are actually much longer than shown here.

observed at the beginning of the first cell division. Babo1 was exclusively found on the two oldest basal bodies and on their MTRs.

Small amounts of Babo1 are detectable in ectosomes above the basal apparatus

Before and during the first cell division, Babo1–YFP was also observed in a pair of tiny dots just above the strong signals at the basal apparatus (Figure 7). The localization of these tiny dots is outside of the plasma membrane within the extracellular matrix (ECM), which raised the question of how Babo1–YFP could get there. It is known that undifferentiated reproductive cells develop short transient flagellar stubs, which are surrounded by the plasma membrane and protrude out of the cell body into the ECM of the gonidial 'vesicle' (Figure 7d) (Kirk, 1998). In addition, it has been shown that the flagella of *C. reinhardtii* release small, protein-filled membrane vesicles, called ectosomes, into the surrounding space and this budding of vesicles frequently happens at the flagellar tips (Wood *et al.*, 2013; Wood and Rosenbaum, 2015). The ectosomes contain both membrane and flagellar proteins and their release appears to be linked to the flagellar resorption (Long *et al.*, 2016).

Taken together, our results indicate that ectosomes with some Babo1–YFP protein are released from the flagellar stubs when these stubs are retracted from the maturing cell. The released ectosomes remain at their initial position within the ECM throughout the first cell division (Figure 7c,f). However, the distance between ectosomes and the basal bodies increases during cell

division because once the cleavage furrow appears and then deepens, the basal bodies move together with the midcell constriction of the plasma membrane. The diameter of the ectosomes is roughly about 50–200 nm and this number is in accordance with earlier reports in *C. reinhardtii* (Wood *et al.*, 2013).

Babo1–YFP uncovers variations of basal apparatus morphology in maturing reproductive cells

Because Babo1–YFP stains significant parts of the basal apparatus, it allows the study of the morphology of the basal apparatus in more detail. As *Volvox* cultures can be maintained in synchronous growth and development under an 8 h dark/16 h light regime, synchronized individuals can be easily compared with each other. The structure of the basal apparatus was found to be very variable in reproductive cells at the stage shortly before onset of the first cell division (Figure 8). In some reproductive cells, a prominent central axis was visible (see arrows in Figure 8a). The number of fluorescent strands in one optical section of the CLSM varied greatly from three to six. In the course of the transition from interphase to mitosis, the microtubular cytoskeleton undergoes major structural rearrangements and the probasal bodies elongate into mature basal bodies (Gould, 1975). The observed variations in basal apparatus morphology are presumably linked to these processes.

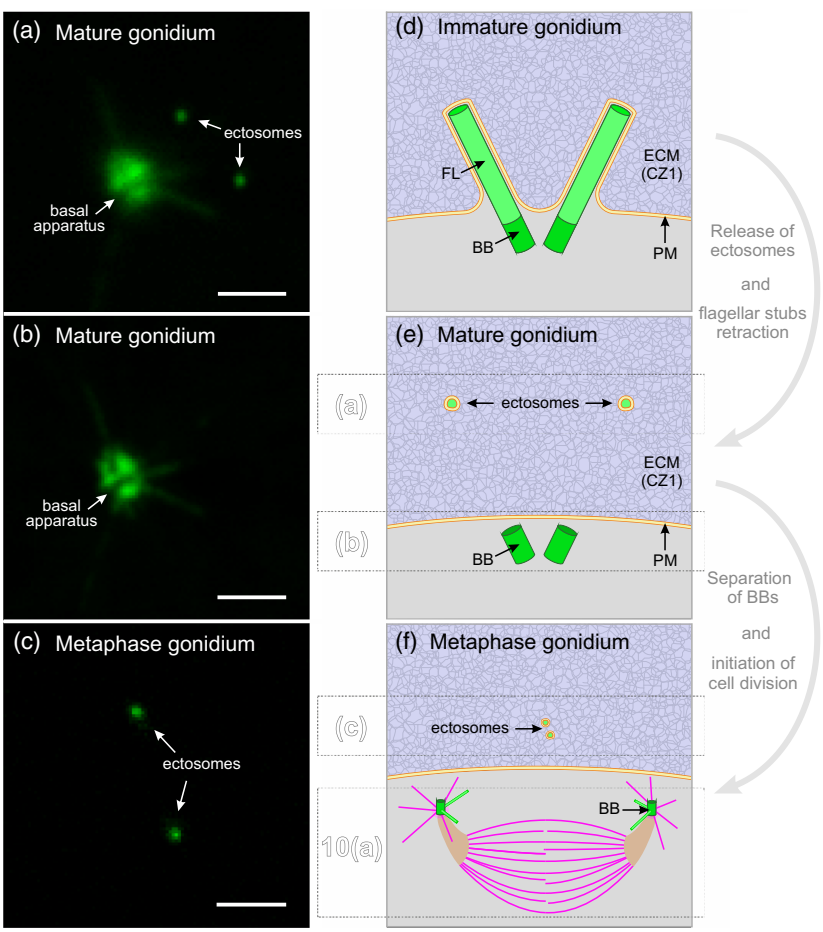

Figure 7. Babo1–YFP localization in ectosomes above the basal apparatus of gonidia. (a) Shortly before the first cell division, a small amount of Babo1–YFP (green) was localized in a pair of ectosomes above the basal bodies, in addition to its localization in the lumen of the basal bodies and at the MTRs. The basal apparatus is also visible but appears blurry because it is localized below the focal plane. The viewing direction is from outside obliquely onto the surface of the gonidium. (b) Same mature gonidium and same viewing direction as in (a) but in this image the basal apparatus is in the focal plane. (c) Top view onto the area above the basal apparatus of a metaphase gonidium expressing Babo1–YFP. The ectosomes are in the focal plane, whereas the basal bodies and the spindle are located deeper inside the cell. The basal bodies and spindle of this gonidium are shown in Figure 10(a). (a–c) *In vivo* CLSM images. Scale bars = 2 μm. (d–f) Schematic depiction of the localization of ectosomes in side view. The focal planes of the images in (a–c) are indicated. The position of the Z-stack in Figure 10(a) is also shown. PM, plasma membrane; BB, basal body; FL, flagellar stubs; ECM, extracellular matrix. (d) Immature gonidium. Flagellar stubs protrude out of the cell into the ECM of the gonidial 'vesicle', which corresponds to the cellular zone 1 (CZ1) of the ECM (Kirk *et al.*, 1986; Hallmann, 2003). (e) Mature gonidium. Ectosomes have been released at the tips of the flagellar stubs before or during retraction of the flagellar stubs. (f) Metaphase gonidium. The ectosomes persist in the ECM while the basal bodies separate from each other and cell division is initiated. The viewing directions of images in (d–f) (side view) are roughly perpendicular to the viewing directions of images (a–c) (top view).

When the first cell division approached, the Babo1–YFP signal was more concentrated at the two basal bodies, the fluorescent strands were hardly visible and a very distinct central axis was present in all cells (Figure 8b). Immediately before the two basal bodies separated from each other, the central axis disappeared and the four strands of rootlet microtubules became clearly visible (Figure 8c). At this developmental stage, the basal apparatus clearly showed point symmetry, as known from other species (Melkonian, 1978). The d-roots formed a straight line, whereas the s-roots were slightly displaced against each other. The Babo1–YFP signal appeared clearly brighter on the d-roots than on the s-roots (Figure 6f). This distribution is similar to the position of the SMAFs in *C. reinhardtii*, which are thicker on the d-roots and less pronounced on the s-roots (Geimer and Melkonian, 2004).

Babo1–YFP allows the monitoring of basal body separation during prophase

During prophase, the basal bodies separate from each other and the MTRs remain attached to their respective basal body. Babo1–YFP is again localized predominantly at the basal bodies and the two-membered d-roots (Figure 9). On the four-membered strands of microtubules (s-roots) Babo1–YFP exhibits an irregular, patchy pattern. However, the degree of patchiness on the s-roots varies between different dividing cells (compare Figure 9a–i,k). During the separation of basal bodies, the s-roots slide along each other and the basal bodies with their associated microtubular roots exhibit a clockwise rotation (Figure 9a–i). The basal bodies also move slightly with the midcell constriction of the plasma membrane into the cleavage furrow, as is indicated by the changing chlorophyll signal of the chloroplast. At first, the s-roots slide along each other with a parallel movement while keeping a distance of approximately 0.5 μm between each other (Figure 9c). Later, they gradually come closer together (Figure 9d–f) until the s-roots contact each other (Figure 9g). Initially, the angle by which the s-root and the d-root are connected to the corresponding basal body measures approximately 100° (Figure 9a). During the movement it widens to approximately 150° coinciding with a significant curvature of the MTRs (Figure 9a–h). The idealized overlay in Figure 9(j) summarizes the movements of both basal bodies with their associated MTRs.

During the separation of the basal bodies, their distance increases continuously from approximately 1 μm (Figure 9a) to approximately 8.7 μm (Figure 9i). In Figure 9(k), which shows the separation shortly after that in Figure 9(i), the distance reached approximately 9.7 μm. Later, during formation of the spindle, the distance grew to approximately 13.4 μm (see Figure 10a).

Localization of Babo1 during spindle and phycoplast formation

Later in cell division when the mitotic spindle forms, the spindle poles are localized somewhat below the MTOCs (Figure 10). Babo1–YFP is still localized at the basal bodies, on the d-roots and, to a lesser extent, on the s-roots. The dark area between the MTOC and the spindle pole (Figure 10a7) most probably corresponds to the nucleus–basal body connector (NBBC). During cytokinesis, the basal bodies with their associated MTRs are localized above the newly formed nuclei and close to the leading edge of the emerged division furrow (Figure 10b). At this stage, the d-roots are almost parallel to the division furrow, whereas the s-roots are roughly perpendicular to the division furrow (Figure 10b2). Figure 10(c,d) schematically shows top and side views of the cell division apparatus during metaphase to better illustrate the three-dimensional arrangements and spatial relationships of the basal bodies, MTOC, MTRs, and spindle. Remarkably, the new mature basal bodies, which must have reached their full length before basal body separation, did not show any Babo1–YFP fluorescence. The same applies to the d- and s-roots of the new basal bodies. Later in the two-celled embryos, when the first division was completed, the Babo1–YFP fluorescence was still limited to the oldest basal bodies and their roots. Neither the probasal bodies, nor the newly formed mature basal bodies, nor any of their corresponding MTRs contained detectable amounts of Babo1–YFP. Apparently, during and after the first cell division, no new Babo1–YFP was synthesized.

Distribution of Babo1 in four-celled embryos

Even after the second cell division, Babo1–YFP was exclusively found on the oldest basal bodies of the four-celled embryo and on the corresponding d-roots (Figure 11). The position of the basal bodies and the orientation of the d-roots are typical for this developmental stage. Also during the second cell division no new Babo1–YFP was expressed and, thus, only two of the four cells contained Babo1–YFP. Again, neither the probasal bodies nor the newly formed mature basal bodies nor any of their corresponding MTRs showed Babo1–YFP fluorescence. All focal planes of four-celled embryos were repeatedly investigated to confirm this result. Thus, we were able to prove that there is an unequal protein distribution among the cells of a four-celled *Volvox* embryo.

Because the overall signal intensity of Babo1–YFP decreased during the progression of embryogenesis, we were not able to clearly monitor the localization of Babo1–YFP after the third cell division. Thus, Babo1–YFP either could be gradually degraded in these later embryonic stages or it could gradually detach from the basal bodies

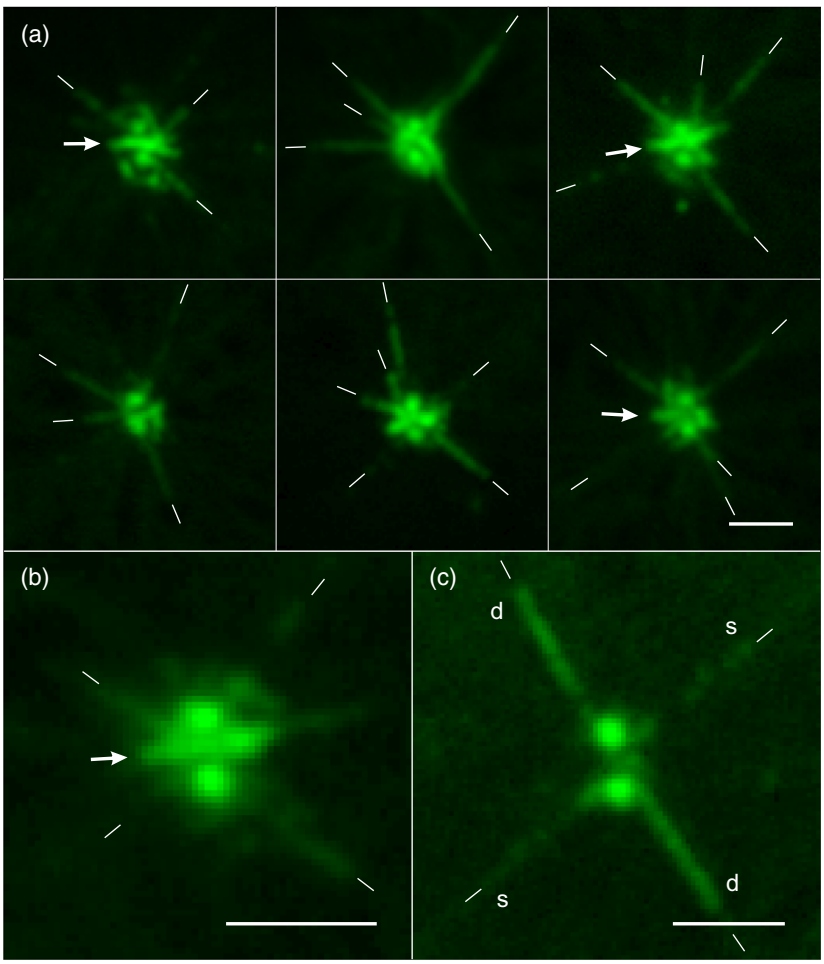

Figure 8. Babo1–YFP highlights the basal apparatus morphology of maturing gonidia. Maturing gonidia of Babo1–YFP transformants were analyzed for basal apparatus morphology. The strongest Babo1–YFP fluorescence (green) localizes to the two circular-shaped basal bodies. In addition, strands of Babo1–YFP fluorescence protrude radially from the basal apparatuses. (a) The six images of Babo1–YFP localization in gonidia illustrate the diversity in morphology approximately 1 h before the first cell division. (b) Shortly before the first cell division begins, basal apparatus morphology in gonidia eventually becomes harmonized. (c) Immediately before the basal bodies are separated from each other, the appearance of the basal apparatus is almost perfectly point-symmetrical. Note that the d-roots appear brighter than the s-roots, which correlates with thicker SMAFs on the d-roots (see Figure 6f). s, s-root; d, d-root. (a, b) Some basal apparatuses show a central axis (arrow), which is perpendicular to an imaginary line connecting the basal bodies. (a–c) *In vivo* CLSM images. The viewing direction is from outside onto the surface of each gonidium. Scale bars = 2 μm.

and dilution of Babo1–YFP in the cytoplasm might be the reason for the steady decrease of structured fluorescence.

DISCUSSION

Previously supposed opsin characteristics of Babo1

Earlier reports on Babo1 stated that this protein is an opsin that contains not only multiple transmembrane helices but also a conserved retinal-binding domain (Deininger *et al.*, 1995; Ebnet *et al.*, 1999; Fuhrmann *et al.*, 1999; Deininger *et al.*, 2000; Fuhrmann *et al.*, 2001; Fuhrmann *et al.*, 2003; Ozawa *et al.*, 2009; Greiner *et al.*, 2017). To re-examine this statement, we initially performed sequence similarity searches and we were able to identify more than 60 proteins from a wide range of algae species that are clearly related to Babo1. A multiple sequence alignment of the family of Babo1-related proteins demonstrates that the earlier proposed opsin-like retinal binding site of Babo1 (Ebnet *et al.*, 1999) is not conserved. Even after a thorough investigation of the multiple alignment of Babo1-related proteins we could not identify those amino acids positions that are conserved or functionally important for microbial opsins. In addition, no seven transmembrane (7TM) helix core architecture has been identified in Babo1, which would be a decisive part of a rhodopsin. Actually, we were not even able to identify a single transmembrane spanning segment in Babo1 and all of the numerous applied programs predicted that Babo1 is not a transmembrane protein. It is fitting, therefore, that we localized Babo1 away from any membrane structures at the basal bodies. Furthermore, when *C.r.* Babo1 was expressed in *Xenopus* oocytes, it was not found in the membrane fraction (Tian *et al.*, 2018). Given that all rhodopsins known to date have at least seven transmembrane helices and also contain a conserved retinal binding site (Gao *et al.*, 2015), it is obvious that Babo1 is not an opsin. Because binding of [^{3}H]retinal led to the initial identification and purification of Babo1 (Deininger *et al.*, 1995), it is still possible that Babo1 binds retinal by a mechanism and binding site different from known retinal binding proteins. It can be assumed that retinal molecules form Schiff bases with the ε-amino groups of the abundant lysyl residues of Babo1. In this context, it should be noted that retinal binding of Babo1 has only been shown *in vitro* and, thus, its retinal-binding capacity should also be investigated under *in vivo* conditions to exclude possible artifacts.

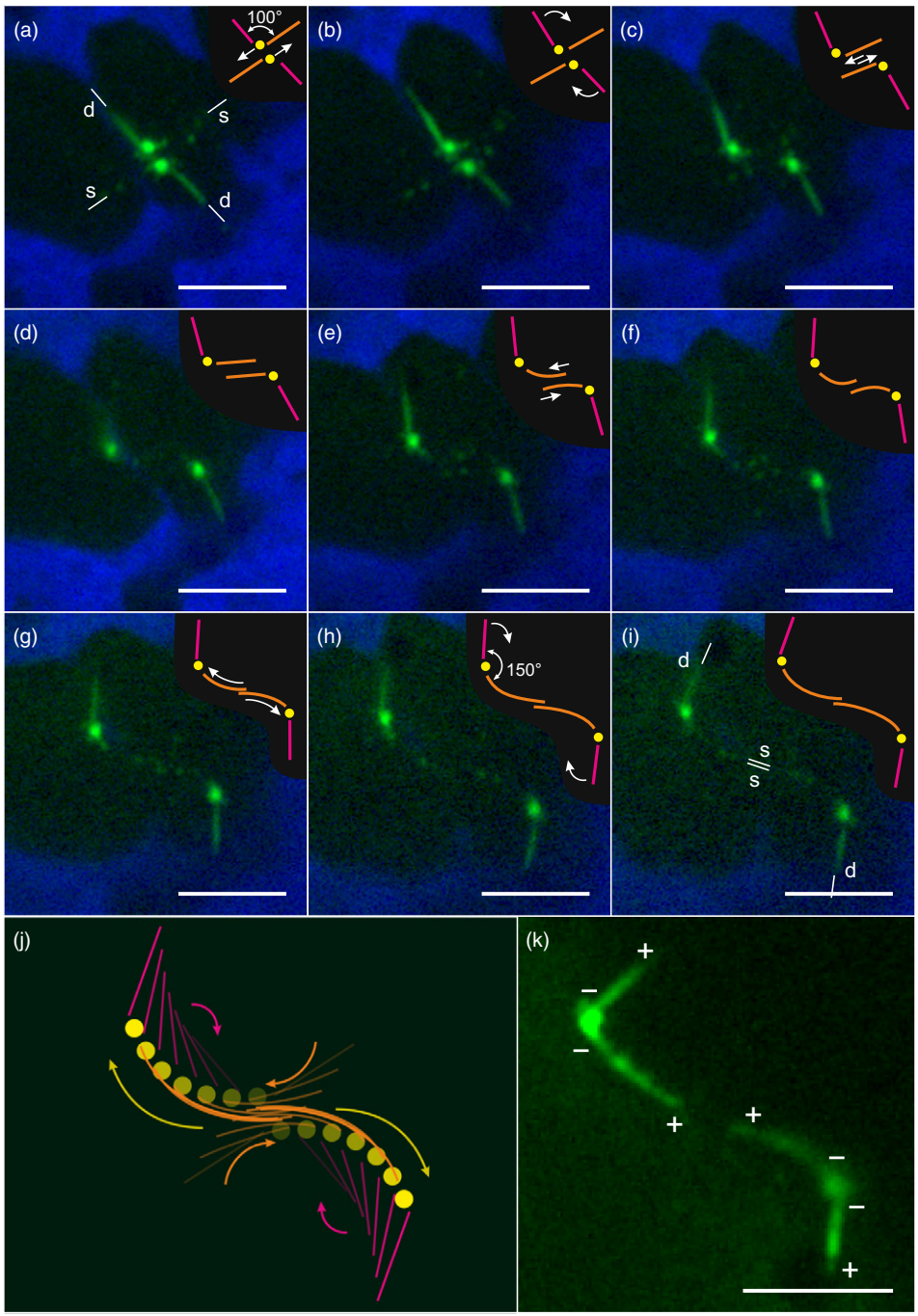

Figure 9. *In vivo* observation of basal body separation in prophase by Babo1–YFP. (a–i) Time-series of *in vivo* CLSM images showing a gonidium expressing Babo1–YFP in the prophase of the first cell division when the two basal bodies with attached MTRs separate from each other. The basal body separation is accompanied by a clockwise rotation of the MTRs. During the separation process, Babo1–YFP (green) is predominantly localized at the basal bodies and on the two-membered MTRs (d-roots). On the four-membered MTRs (s-roots), Babo1–YFP is only detectable to a lesser extent and its distribution appears irregular and patchy. The viewing direction is from outside onto the surface of the gonidium. Chlorophyll (blue) is displayed for orientation. The image sequence covers 15 min. s, s-root; d, d-root. Scale bars = 5 μm. (Insets in a–i) Schematic representation of the situation in (a–i) illustrating the spatial arrangement of basal bodies (yellow), d-roots (magenta) and s-roots (orange). White arrows indicate steady movements between the illustrations. (j) Schematic summary of the sequence shown in (a–i). The transparency is increasingly reduced beginning with the arrangement in (a). Colored arrows indicate the arc-like movements of the basal bodies (yellow) and changing angular positions of their associated d-roots (magenta) and s-roots (orange). (k) *In vivo* CLSM image presenting the appearance of basal bodies with attached MTRs shortly after the sequence shown in (a–i). Plus and minus ends of the microtubular rootlets are indicated. Scale bar = 5 μm.

Previously supposed eyespot localization of Babo1

By analyzing fluorescence spectra, we were able to prove that YFP-tagged Babo1 protein is clearly not localized at the eyespot area, but at the basal bodies. The eyespots of both *babo1*-expressing transformants and wild-type control cells only showed an autofluorescence signal but no YFP signal. Any quenching of Babo1–YFP fluorescence by carotenoid pigments of the eyespot apparatus is virtually impossible because all validated eyespot photoreceptors are located in the plasma membrane above the carotenoid layer (Melkonian and Robenek, 1980; Kreimer, 2009) and our viewing direction was from outside of the *Volvox* spheroid onto the eyespot of the corresponding somatic cell. Furthermore, the performed spectral imaging in lambda mode makes it possible to separate superimposed signals if they exist and, thus, any existing YFP at the eyespot would have been identified and clearly discriminated from the autofluorescence of the eyespot. In the past, technical difficulties in differentiating between reporter fluorescence and autofluorescence seem to have produced misleading *in vivo* localization results regarding Babo1 (Deininger *et al.*, 1995; Fuhrmann *et al.*, 1999). Possible causes might be that in this previous work an earlier, less advanced generation of CLSM devices without spectral imaging detectors was utilized and that Babo1 has previously been tagged with GFP. Unfortunately, eyespots of both *Volvox* and *Chlamydomonas* cells showed a quite high level of background autofluorescence when GFP is excited at its optimal wavelength. By contrast, this autofluorescence does not apply to YFP. In earlier experiments, Babo1 also was detected by FITC-conjugated antibodies using glutaraldehyde-fixed cells (Deininger *et al.*, 1995), whereby glutaraldehyde is known to cause especially high autofluorescence (Lee *et al.*, 2013). Moreover, FITC fluorescence intensity peaks at 541 nm, which strongly overlaps with eyespot autofluorescence. Thus, eyespot autofluorescence also appears to have been misinterpreted as FITC fluorescence.

Even though both previous Babo1 localization studies had made efforts to deal with autofluorescence issues (Deininger *et al.*, 1995; Fuhrmann *et al.*, 1999), it was technically not possible to separate autofluorescence from FITC or GFP fluorescence. The previous incorrect fluorescence-based localization of Babo1 at the eyespot has then been viewed as a confirmation of the circumstances in which Babo1 was originally extracted from eyespot membrane preparations of *V. carteri* and *C. reinhardtii* (Deininger *et al.*, 1995; Ebnet *et al.*, 1999). However, in the knowledge of our results, the presence of Babo1 in any eyespot fractions can also be explained by the fact that the eyespot and the basal bodies are connected with each other by the D4 MTR (Mittelmeier *et al.*, 2015) and, thus, basal bodies could attach to the eyespot or components of it during eyespot isolation. It should also be noted that Babo1 has been identified in several other cellular fractions (Allmer *et al.*, 2006; Goold *et al.*, 2016; Long *et al.*, 2016) and this might indicate that Babo1 tends to bind unspecifically to other cellular components during cell fractionation.

Functional implications of sequence analysis and subcellular localization of Babo1

Our results demonstrate that Babo1 clearly accumulates at the basal apparatus of both somatic and reproductive cells. More precisely, it is located predominantly at the basal bodies and, to a lesser extent, at the four strands of rootlet microtubules. Generally, basal bodies serve as microtubule organizing centers. The building block of a basal body or any microtubule is the tubulin subunit, a heterodimer of α-tubulin and β-tubulin. These tubulins both possess a glutamic acid-rich 'E-hook' at their C-terminal ends and these negatively charged segments protrude out of the microtubule filaments. The E-hooks can be bound by proteins (e.g. kinesins) with positively charged, poly-lysine containing K-loops (Okada and Hirokawa, 2000). In general terms, a high content of positively charged residues is a common feature of microtubule binding motives (Zhou *et al.*, 2015). Markedly, the lysine content of Babo1 is at the considerable value of 17.2%, which corresponds to every sixth amino acid. Furthermore, sequence analysis using the Microtubule-Associated Protein Analyzer (MAPanalyzer) (Zhou *et al.*, 2015) identified six different motifs that are known to be enriched in microtubule binding sites and that are spread over the entire amino acid sequence of Babo1. These findings suggest a direct interaction between Babo1 and the tubulins of microtubules or basal bodies.

In *C. reinhardtii* cells, and in the somatic cells of *Volvox*, basal bodies provide the basis for flagellar assembly because they serve to nucleate the growth of axonemes (Kirk, 1998; Dutcher and O'Toole, 2016). However, knockdown experiments in *C. reinhardtii* suggested that Babo1 is not essential for flagellar function (Fuhrmann *et al.*, 2001). Furthermore, Babo1 of *V. carteri* is clearly overexpressed in the flagella-less reproductive cell-type when compared with the somatic cell-type (Ebnet *et al.*, 1999; Kianianmomeni and Hallmann, 2015; Klein *et al.*, 2017). Those aspects make it unlikely that Babo1 has a relevant role in flagellar assembly, function, or stabilization. The observed overexpression in reproductive cells suggests, however, a role for Babo1 in cell division or cell cycle-associated functions. In fact, basal bodies are related to metazoan centrioles, which aid in mitosis and nucleate and organize the centrosomes. Basal bodies and related centrioles are also known to be an important signaling center of the cell (Arquint *et al.*, 2014; Loncarek and Bettencourt-Dias, 2018). Basal bodies of *C. reinhardtii* are also known to be relevant for the spatial and temporal coordination of karyokinesis and cytokinesis. Mutants of

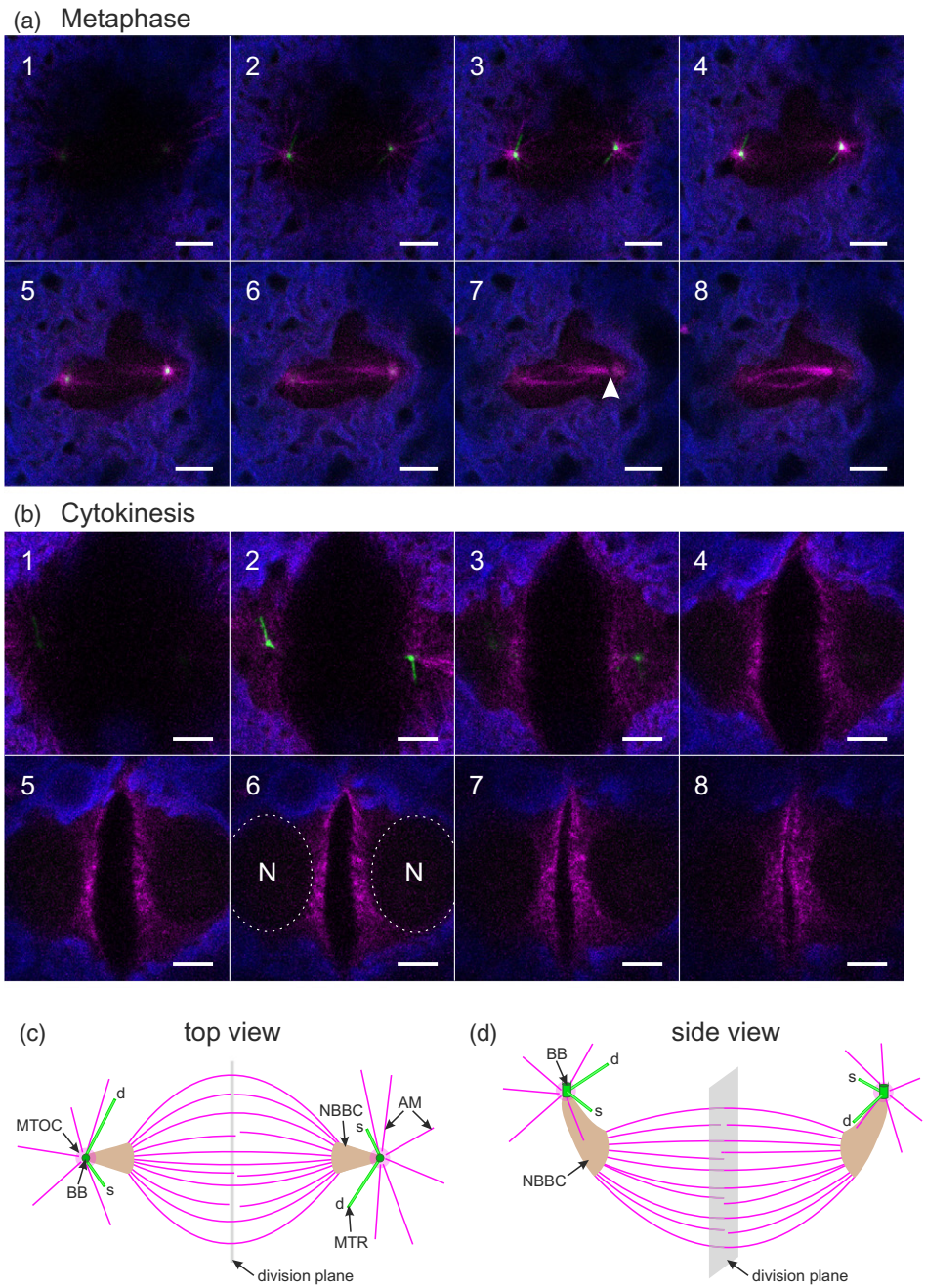

Figure 10. Topology of the Babo1–YFP localization relative to MTOC, spindle and division furrow. (a, b) Z-stack of a Babo1–YFP expressing gonidium in metaphase (a) and during cytokinesis (b). *In vivo* CLSM images displaying the localization of Babo1–YFP (green), TubB2-CFP (magenta) and chlorophyll (blue). The viewing direction is from outside onto the surface of the gonidium. Scale bars = 5 μm. (a) Gonidium during the metaphase of the first cell division. The distance between the Z-layers is approximately 0.7 μm. The basal bodies and MTRs are localized at the MTOC, which is localized slightly above the spindle poles. The unstained region between the MTOC and the spindle pole in (a7) (see arrowhead) corresponds to the location of the nucleus–basal body connector. (b) Gonidium during cytokinesis of the first cell division. The basal bodies with their associated MTRs are located at the edge ('shoulder') of the division furrow, right above the newly formed nuclei (dashed lines in b6). The d-roots are almost parallel to the division furrow and the hardly visible s-roots are roughly perpendicular to the division furrow. The distance between the Z-layers is approximately 1.7 μm. (c, d) Schematic depiction of the cell division apparatus in metaphase showing basal bodies (BB, dark green), microtubular rootlets (MTR, light green), astral and other microtubules (AM, magenta), microtubule-organizing centers (MTOC, light magenta) and the nucleus–basal body connectors (NBBC, brown). (c) Top view. (d) Side view. s, s-root; d, d-root.

C. reinhardtii that lack basal bodies are not able to determine the right time and place for formation of the spindle and the division furrow (Ehler *et al.*, 1995). Thus, Babo1 could play a critical role in influencing such processes. Our subcellular tracking of Babo1 during the first cell divisions showed that Babo1 is only present on the

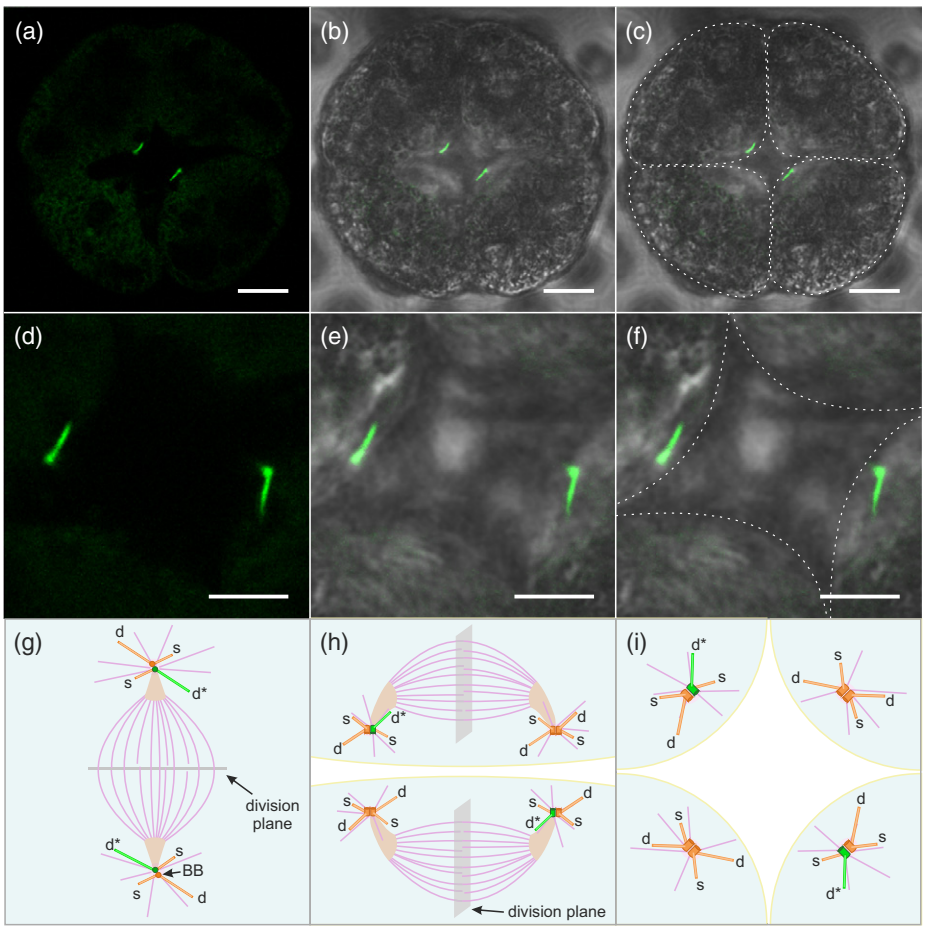

Figure 11. *In vivo* localization of Babo1–YFP in four-celled embryos. (a–c) Overview of a four-celled *Volvox carteri* embryo expressing Babo1–YFP. The viewing direction is from outside onto the surface of the embryo. (d–f) Zoomed view onto the central part of a four-celled *V. carteri* embryo. (a, d) Babo1–YFP fluorescence. (b, e) Overlay of Babo1–YFP-signal and transmitted light detected by a photomultiplier tube (trans-PMT). (c, f) Same as in (b) and (e) but with additional dashed lines indicating the approximate positions of the cell boundaries. (a–f) The Babo1–YFP fluorescence is found only in two opposing cells of the four-celled embryo and within these two cells it is localized exclusively at the older basal bodies and their associated d-roots. Note that each of these cells actually contains two basal bodies and four MTRs, but only components with Babo1–YFP fluorescence are visible. (a–c) Scale bars 10 μm. (d–f) Scale bars 5 μm. (g–i) Schematic depiction of the basal apparatuses viewed from outside onto the surface of the gonidium. The two oldest basal bodies with their respective d-roots are associated to Babo1–YFP and are shown in green. Basal bodies and microtubular roots that show no fluorescence are shown in orange. The two oldest s-roots lose fluorescence between the first and the second cell division. (g) First mitosis. (h) Second mitosis. (i) Four-celled embryo after the second cell division. BB, basal body; s, s-root; d, d-root; d*, d-root associated with Babo1–YFP. Other structures are described in Figure 10.

oldest basal bodies and on the corresponding d-roots. Four-celled embryos therefore show an unequal allocation of Babo1: Only two of the four cells contained Babo1–YFP-stained basal bodies and d-roots. This finding demonstrates a controlled temporal and unequal spatial distribution of Babo1 in dividing embryos.

The structure, regulation, and inheritance pattern of basal bodies and related centrioles is conserved in all branches of the eukaryotic tree of life, from unicellular algae all the way to mammals (Holmes and Dutcher, 1989; Wang *et al.*, 2009). In multicellular organisms, the strict allocation of these structures during division therefore offers a suitable option for unequal distribution of attached cellular components among daughter cells, which leads to asymmetric cell division and, finally, to different cell types (Nigg and Stearns, 2011). For example, when mammalian centrioles separate in embryonic divisions, a centrosome-based mechanism is responsible for asymmetric distribution of certain proteins between daughter cells (Fuentealba *et al.*, 2008). Due to the controlled temporal and unequal, spatial distribution of Babo1 in four-celled embryos, Babo1 could serve as a marker for asymmetry at this early stage of embryonic development. The relevance of Babo1 for proper embryogenesis of *V. carteri* is also supported by the characteristics of a transgenic strain with knocked-down expression of *babo1.* The corresponding algae grew and divided only slowly and their division pattern has been described as totally uncoordinated (Ebnet *et al.*, 1999).

In view of the unequal distribution of Babo1, it might also be crucial that Babo1 has the capacity to bind retinal (Kröger and Hegemann, 1994; Deininger *et al.*, 1995). In vertebrates, retinal derivatives such as retinol and retinoic acid are well known signaling molecules that play a major role in embryogenesis. During embryonic development, a concentration gradient of retinoic acid is established along the body axis (Shimozono *et al.*, 2013) that is essential for correct patterning of embryos (Niederreither and Dolle, 2008). In a close relative of *Volvox*, *C. reinhardtii*, the presence of endogenous retinal has been demonstrated (Beckmann and Hegemann, 1991). Furthermore, this alga can convert retinal into retinol, which was assumed to be a storage form of retinal (Beckmann and Hegemann, 1991). The reaction is catalyzed by retinol dehydrogenases and our genome searches confirmed that also *V. carteri* (Prochnik *et al.*, 2010) has potential retinol dehydrogenase genes. At least one of these genes is well transcribed based on RNA-seq data (Klein *et al.*, 2017). For conversion of retinal into retinoic acid, a retinal oxidase is required. Two potential retinal oxidase genes have been identified in the *V. carteri* genome and at least one of these genes is well transcribed (Klein *et al.*, 2017). We also identified a well transcribed but yet unannotated gene, Vocar.0007s0453, which codes for a protein that shows similarity to the human retinoic acid induced protein 1. Thus, retinoids seem to be relevant for *Volvox*. If the concentration of retinoids in dividing *Volvox* embryos is decisive for the cell fate, Babo1 could be responsible for the unequal distribution of these retinoids.

Morphology of the basal apparatus and *in vivo* observation of basal-body separation

Both the morphology of the basal apparatus and the separation process of basal bodies or centrioles are significant fields of research in cell biology, in particular as numerous disorders are associated with centriolar, centrosomal, or ciliary dysfunctions (Chavali *et al.*, 2014; Nigg *et al.*, 2014; Kempeneers and Chilvers, 2018; Schatten and Sun, 2018; Wang and Dynlacht, 2018). Because Babo1 co-localizes with basal bodies and rootlet microtubules, Babo1–YFP can be utilized as a fluorescent stain for *in vivo* investigation of these cellular structures. Our method and equipment allow not only for high-resolution *in vivo* imaging of the fine structures of the basal apparatus but also for *in vivo* tracing of their developmental dynamics. By contrast, many previously used methods require chemical fixation, dehydration, cutting, and staining. Dyes may infiltrate insufficiently or can potentially interfere with the specimen and cause experimental artifacts. Immunostaining with antibodies conjugated with fluorescent ligands is also an error-prone method. Moreover, these earlier methods provided only a snapshot of the dynamic developmental processes and they did not allow continuous following of the fate of one and the same cell and its components. Basal-body separation of *V. carteri* embryos has never been observed *in vivo* before and the observations in the related unicellular alga *C. reinhardtii* did not reach our temporal and optical resolution (Kirk *et al.*, 1991; Kirk, 1998; Lechtreck *et al.*, 2002). Our results also show that Babo1–YFP forms a prominent central axis between the two basal bodies just before first basal body separation. Although there are several investigations of basal bodies in *C. reinhardtii* (Dutcher and O'Toole, 2016), this structure has not been reported previously. One reason why it remained undiscovered could be that the structure is detectable only for a very short period of time. We were also able to show that the angle, in which the two microtubular rootlets are connected to the corresponding basal body, widens from approximately 100° to approximately 150° during separation of basal bodies. This is probably attributable to the force that is applied to the rootlets at the regions where the two s-roots come close together and are likely to touch each other. We assume that this force pushes the basal bodies away from each other and it might also be sufficient to induce rotational movement.

CONCLUSION

The protein Babo1 (formerly Vop1 or Cop1/2) has previously been classified as an eyespot-photoreceptor, but is neither localized at the eyespot nor is it an opsin. It is not even a transmembrane protein. We revealed a large family of more than 60 Babo1-related proteins from a wide range of algae species and showed their relationship in a molecular phylogenetic analysis. Our high-resolution *in vivo* imaging demonstrates that Babo1 is localized at the basal bodies and, to a lesser extent, at the four strands of rootlet microtubules. Dynamic structural rearrangements of Babo1 particularly occur right before the first cell division. In four-celled embryos, Babo1 was exclusively found on the two oldest basal bodies of the embryo and on the corresponding d-roots. The coordinated asymmetric distribution of Babo1 in four-celled embryos is the first molecular evidence for differences in protein composition among cells of such a very early stage of embryonic development in *V. carteri*. The spatial and temporal distribution of Babo1, therefore, suggests a role in cell division. The unequal distribution of Babo1 in four-celled embryos could be an integral part of a geometrical system in early embryogenesis, which establishes the anterior–posterior polarity and influences the spatial arrangement of embryonic structures and characteristics. Due to its retinal-binding capacity, Babo1 could also be responsible for the unequal distribution of retinoids, knowing that concentration gradients of retinoids can be essential for the correct patterning of

embryos. Our findings, therefore, push Babo1 research in another direction and provide a promising basis for functional analyses.

EXPERIMENTAL PROCEDURES

Strains and culture conditions

The wild-type *Volvox carteri f. nagariensis* strain Eve10 (female) (Starr, 1969; Starr, 1970; Adams *et al.*, 1990; Kianianmomeni *et al.*, 2008), which originates from Japan, was used to produce a nitrate-reductase deficient (*nit*A$^-$) descendant for transformation experiments. The nitA$^-$ descendant of Eve10 was generated by random mutagenesis and chlorate selection as previously described (Huskey *et al.*, 1979; Harper *et al.*, 1987; Adams *et al.*, 1990). The obtained non-revertible mutant strain, TNit-1013 (Tian *et al.*, 2018), contains a deletion of 1013 bp in the *nit*A gene and, therefore, is not able to grow in medium containing nitrate as the sole source of nitrogen. *V. carteri* strain TNit-1013 was therefore grown in *Volvox* medium (Provasoli and Pintner, 1959; Starr, 1969) supplemented with 1 mM ammonium chloride (NH_4Cl) as a nitrogen source. Strain Eve10 was grown in standard *Volvox* medium (Provasoli and Pintner, 1959; Starr, 1969). Transformation and CLSM analyses required synchronization of development of *Volvox* cultures that was achieved by growth under a light–dark cycle. Synchronous cultures were grown at 28°C in a cycle of 8 h dark/16 h cool fluorescent white light (Starr and Jaenicke, 1974) at an average of approximately 100 μmol photons m^{-2} sec^{-1} photosynthetically active radiation. Cultivation was performed in glass tubes with caps that allow for gas exchange or in Fernbach flasks, which were aerated with approximately 50 cm^3 sterile air/min. For synchronous growth, culture density was no more than 10 spheroids/ml.

Construction of vectors for expression of fusion proteins in *V. carteri*

For construction of expression vectors carrying the *V.c. babo1* gene (Vocar.0024s0227) fused to the *yfp* reporter gene (plasmid pBlue_Babo1_YFP; Figure 3a) and the *cfp* reporter gene fused to *tubB2* (Vocar.0007s0229) (plasmid pBlue_CFP_TubB2; Figure 3c), recombinant PCRs were performed using the oligonucleotides shown in Table S3 as primers and both genomic DNA of *V. carteri* and plasmids carrying *yfp* or *cfp* genes as a template. The amplified PCR products were assembled within pBluescript II SK(−) (Stratagene) vector backbones. Both *yfp* (mVenus) (Kremers *et al.*, 2006) and *cfp* (mCerulean3) (Markwardt *et al.*, 2011) were previously engineered to match the codon usage of *C. reinhardtii* (Lauersen *et al.*, 2015). On plasmid pBlue_Babo1_YFP, expression of *babo1* is driven by the endogenous *babo1* promoter. The corresponding DNA fragment is 215 bp in size, ends 15 bp upstream of the *babo1* start codon, contains the remaining 33 bp of the 5′UTR and is flanked by artificial *Kpn*I and *Apa*I sites (Figure 3a). The *babo1* start codon is preceded by a 6-bp Kozak sequence. A 1959-bp *babo1* genomic fragment with all introns included (artificial *Apa*I to artificial *Eco*RV; Figure 3a) was amplified in two parts (*Apa*I to *Xho*I and *Xho*I to *Eco*RV; Figure 3a) making use of an endogenous *Xho*I site. Artificial *Eco*RV sites were added on both sides of the intronless *yfp* and, simultaneously, a short linker sequence, which codes for a flexible pentaglycine interpeptide bridge, was inserted in front of the *yfp* gene (0.7 kb, *Eco*RV to *Eco*RV; Figure 3a). The utilized *babo1* terminator region is within a 1-kb fragment (artificial *Eco*RV to artificial *Bam*HI; Figure 3a) containing 0.9 kb of 3′UTR and 100 bp of downstream sequence. In plasmid pBlue_CFP_TubB2, expression of *tubB2* is driven by the endogenous *tubB2* promoter. The corresponding DNA fragment is 462 bp in size, ends 19 bp upstream of the start codon, contains the remaining 99 bp of 5′UTR, and is flanked by two artificial *Xho*I sites (Figure 3c). The artificial *Xho*I site in front of the start codon is immediately (after 1 bp) followed by an artificial *Cla*I site. To facilitate cloning, artificial *Cla*I sites were added on both sides of *cfp* and, simultaneously, a short linker sequence, which codes for a flexible pentaglycine interpeptide bridge, was inserted behind the *cfp* gene (0.7 kb, *Cla*I to *Cla*I; Figure 3c). The *cfp* start codon is preceded by a 6-bp Kozak sequence. A 1879-bp *tubB2* genomic fragment with all introns included was amplified (artificial *Cla*I to artificial *Bam*HI, Figure 3c) and used for vector construction. The terminator region comes from the *V. carteri LHCBM1* gene (Vocar.0001s0479) and is localized within a 0.3-kb fragment (artificial *Xba*I to artificial *Not*I; Figure 3c) containing 173 bp of the 3′UTR and 116 bp of downstream sequence.

Both fusion proteins were additionally brought under control of the LHCBM1 (Vocar.0001s0479) promoter (Figure 3b,d). The *LHCBM1* gene is a chlorophyll *a*/*b* binding protein in the light-harvesting complex II. In previous RNA-seq studies, the LHCBM1 promoter demonstrated strong expression and the expression levels were similar in both cell types (Klein *et al.*, 2017; Tian *et al.*, 2018). A 0.9 kb DNA fragment containing the LHCBM1 promoter region was introduced in front of the fused genes using *Kpn*I/*Apa*I for *babo1*/*yfp* and *Xho*I/*Xho*I for *cfp*/*tubB2*, resulting in the plasmids pBlue_LHCBM1_Babo1_YFP (Figure 3b) and pBlue_LHCBM1_CFP_TubB2 (Figure 3d).

Stable nuclear transformation of *V. carteri*

The *nit*A$^-$ *V. carteri* strain TNit-1013 (Tian *et al.*, 2018) was grown on a larger scale in *Volvox* medium supplemented with 1 mM NH_4Cl. In preparation of particle bombardment, 3 mg of gold microprojectiles (1.0 μm in diameter, Bio-Rad, Hercules, CA, USA) were coated as previously described (Lerche and Hallmann, 2009; Lerche and Hallmann, 2013) using 5 μg of plasmid pVcNR15 (Gruber *et al.*, 1996), which allows for expression of the *nit*A gene for selection, and 5 μg of each plasmid that expresses fused gene constructs for subcellular localization (Figure 3). The DNA-coated microprojectiles were suspended in 60 μl ethanol and kept at 4°C for use within 1 h. About 24 000 spheroids of strain TNit-1013 were harvested on a 40-μm stainless steel mesh and washed thoroughly with 3 L of standard *Volvox* medium, which lacks NH_4Cl and, therefore, allows the selection of *nit*A$^+$ transformants. Transformation was performed using a Biolistic PDS-1000/He particle gun (Bio-Rad). The transformation procedure was as previously described (Schiedlmeier *et al.*, 1994; Hallmann and Wodniok, 2006; Lerche and Hallmann, 2009; Lerche and Hallmann, 2013; Lerche and Hallmann, 2014), with the subsequent modifications. One-sixth of the suspension with DNA-coated microprojectiles (10 μl) was evenly spread on a macrocarrier (Bio-Rad) that was placed in a macrocarrier holder (Bio-Rad). The ethanol was allowed to evaporate from the surface of the macrocarrier. The burst pressure of the rupture disks was 900 psi, the rupture disk–macrocarrier distance was adjusted to 7 mm, the macrocarrier-stopping screen distance was 8 mm, the stopping screen-target cell distance was 11 cm, and the bombardment chamber was evacuated to 28 inches of mercury. After each bombardment, the algae were briefly immersed in standard *Volvox* medium. The bombardment procedure was performed six times in total. The algae were then incubated in ammonium-free standard *Volvox* medium under standard conditions. From the fifth day on after particle bombardment, algae cultures were examined for green

and living transformants (*nit*A$^+$) on a background of numerous bleaching, unaltered organisms (*nit*A$^-$). Each identified transformant was transferred to fresh selective medium for further culture. Aside from the expression of *nit*A, expression of the co-transformed fused gene constructs was verified by fluorescence microscopy.

Confocal laser scanning microscopy

For life cell imaging, algae were synchronously grown under standard conditions and examined using an inverted LSM780 confocal laser scanning microscope (Carl Zeiss GmbH, Germany) equipped with a 63× LCI Plan-Neofluar objective (Carl Zeiss GmbH). The confocal pinhole diameter was set to 1 Airy unit, which corresponds to an optical section of 0.8 μm. The YFP fluorescence was excited using an argon ion (Ar$^+$) laser at 514 nm and the emitted fluorescence was detected at 517–553 nm. The CFP fluorescence was excited by a diode laser (Diode 405-30) at 405 nm and the emitted fluorescence was detected at 460–500 nm. Chlorophyll fluorescence also was excited by the diode laser at 405 nm and detection was at 651–700 nm. Fluorescence intensity was recorded in bidirectional scan mode for YFP, CFP, and chlorophyll in three channels simultaneously. Transmission images were obtained in a fourth channel using a transmission-photomultiplier tube (trans-PMT) detector. An incubation device was used to keep the algae suspension on the microscopic slides at 28°C and to prevent evaporation. All images were captured with a bit depth of 12. Images were analyzed using the ZEN black digital imaging software (ZEN 2011, Carl Zeiss GmbH). Image processing and analysis was carried out using Fiji (ImageJ 1.51w) (Schindelin *et al.*, 2012). Figures 6(b), 8, and 9 were gamma adjusted with a value of 0.5–0.7 to improve the overall visibility. The lambda scan function of ZEN and a gallium arsenide phosphide (GaAsP) QUASAR photomultiplier detector (Carl Zeiss GmbH) were used for simultaneous 20-channel readouts. Emission spectra between 517 and 695 nm were recorded for each pixel with a spectral resolution of 8.9 nm using a main beam splitter MBS 458/514 and 514-nm laser light for excitation. After data acquisition, spectral analysis for the regions of interest (ROIs) was performed.

Sequence database search

The TBLASTN and PSI-BLAST algorithms (Altschul *et al.*, 1990; Altschul *et al.*, 1997) were used to search for Babo1-related sequences in the databases of the NCBI, the China National GeneBank (CNGB) and Phytozome 12 (Goodstein *et al.*, 2012). Most hits showing sequence similarity to Babo1 referred to translated transcriptome data produced within the framework of the 1000 plants project (Matasci *et al.*, 2014). Redundant sequences, extremely short sequences and sequences with obvious flaws such as internal stop codons, were excluded from further analyses. However, a few incomplete transcript sequences were completed using genomic data and intron prediction, which was supported by sequence alignments with confirmed Babo1-related sequences. Whenever we found protein isoforms of differing lengths within a certain species, only the longest isoform was chosen for the final protein alignment. A unique, abbreviated protein identifier was assigned to all sequences based on the first three characters of both the genus and the species name (e.g. Volcar for *Volvox carteri*) and the last three digits of either the 1KP scaffold number, the NCBI accession number or the JGI identifier. The final list of Babo1 and Babo1-related proteins and corresponding identifiers is shown in Table S4.

Phylogenetic analysis

The protein sequences were aligned using the MUltiple Sequence Comparison by Log-Expectation program (MUSCLE) (Edgar, 2004). Minor manual optimization of the alignments, trimming, and management of multialigned data was done using BioEdit v7.0.5.3 (Hall, 1999). The alignments were illustrated using GeneDoc 2.7 (Nicholas *et al.*, 1997). The unrooted phylogenetic tree was calculated using the PHYLogeny Inference Package (PHYLIP) (Felsenstein, 1989). In these calculations, 10 000 bootstrap resamplings of multiply aligned sequences were generated using Seqboot. Distance matrices using Dayhoff's point accepted mutation (PAM) were computed with Protdist, trees were constructed using the neighbor-joining method (Saitou and Nei, 1987) as implemented in Neighbor, and finally, a consensus tree was built using Consense. Phylogenetic trees were drawn with iTOL 4.2 (Letunic and Bork, 2016).

Calculation of amino acid composition

Amino acid compositions were calculated for all available protein sequences in the proteomes of *V. carteri* and *C. reinhardtii*, as well as for the Babo1-related proteins shown in Figure 2 and Table S4. Proteome data refer to *V. carteri* v2.1 (Prochnik *et al.*, 2010) and *C. reinhardtii* v5.5 (Merchant *et al.*, 2007) in Phytozome 12 (Goodstein *et al.*, 2012). The compositions of amino acids were calculated using the composition based protein identification (COPId) program (Kumar *et al.*, 2008).

ACKNOWLEDGEMENTS

We are grateful to Thorsten Seidel for support with the CLSM, Saskia Bertsch, and Julia Schröder for cloning of preliminary versions of constructs, Yannic Kerkhoff for preliminary CLSM experiments, Olaf Kruse, Kyle J. Lauersen and Thomas Baier for providing the codon adapted *yfp* and *cfp*, Benjamin Klein for inspiring discussions and Kordula Puls for technical assistance. This work was supported by Bielefeld University.

AUTHOR CONTRIBUTIONS

EH and AH conceived and designed the approach. EH performed and conducted the experiments and analyses in coordination with AH. Both authors wrote the manuscript and approved the final version.

CONFLICT OF INTEREST

The authors declare that they have no conflict of interests.

DATA STATEMENT

All data referred to are included in this article or its Supporting Information files. Plasmids are available upon request.

SUPPORTING INFORMATION

Additional Supporting Information may be found in the online version of this article.

Figure S1. The *V. carteri babo1* gene and its comparison with previous *babo1* variants.

Figure S2. Amino acid composition of Babo1, Babo1-related protein groups, and the proteomes of *V. carteri* and *C. reinhardtii*.

Figure S3. Sequence alignment of Babo1-related proteins.

Table S1. List of the most lysine-rich proteins of *V. carteri*.

Table S2. List of the most lysine-rich proteins of *C. reinhardtii*.

Table S3. List of oligonucleotide primers used for construction of expression vectors.

Table S4. List of Babo1 and Babo1-related proteins.

REFERENCES

Adams, C.R., Stamer, K.A., Miller, J.K., McNally, J.G., Kirk, M.M. and Kirk, D.L. (1990) Patterns of organellar and nuclear inheritance among progeny of two geographically isolated strains of *Volvox carteri*. *Curr. Genet.* **18**, 141–153.

Allmer, J., Naumann, B., Markert, C., Zhang, M. and Hippler, M. (2006) Mass spectrometric genomic data mining: Novel insights into bioenergetic pathways in *Chlamydomonas reinhardtii*. *Proteomics*, **6**, 6207–6220.

Altschul, S.F., Gish, W., Miller, W., Myers, E.W. and Lipman, D.J. (1990) Basic local alignment search tool. *J. Mol. Biol.* **215**, 403–410.

Altschul, S.F., Madden, T.L., Schäffer, A.A., Zhang, J., Zhang, Z., Miller, W. and Lipman, D.J. (1997) Gapped BLAST and PSI-BLAST: a new generation of protein database search programs. *Nucleic Acids Res.* **25**, 3389–3402.

Arquint, C., Gabryjonczyk, A.M. and Nigg, E.A. (2014) Centrosomes as signalling centres. *Philos. Trans. R. Soc. Lond. B Biol. Sci.* **369**, 20130464.

Beckmann, M. and Hegemann, P. (1991) In vitro identification of rhodopsin in the green alga *Chlamydomonas*. *Biochemistry*, **30**, 3692–3697.

Bernhofer, M., Kloppmann, E., Reeb, J. and Rost, B. (2016) TMSEG: novel prediction of transmembrane helices. *Proteins*, **84**, 1706–1716.

Cao, B., Porollo, A., Adamczak, R., Jarrell, M. and Meller, J. (2006) Enhanced recognition of protein transmembrane domains with prediction-based structural profiles. *Bioinformatics*, **22**, 303–309.

Carmel, L. and Koonin, E.V. (2009) A universal nonmonotonic relationship between gene compactness and expression levels in multicellular eukaryotes. *Genome Biol. Evol.* **1**, 382–390.

Chavali, P.L., Putz, M. and Gergely, F. (2014) Small organelle, big responsibility: the role of centrosomes in development and disease. *Philos. Trans. R. Soc. Lond. B Biol. Sci.* **369**, 20130468.

Combet, C., Blanchet, C., Geourjon, C. and Deléage, G. (2000) NPS@: network protein sequence analysis. *Trends Biochem. Sci.* **25**, 147–150.

Cserzo, M., Eisenhaber, F., Eisenhaber, B. and Simon, I. (2004) TM or not TM: transmembrane protein prediction with low false positive rate using DAS-TMfilter. *Bioinformatics*, **20**, 136–137.

Deininger, W., Kröger, P., Hegemann, U., Lottspeich, F. and Hegemann, P. (1995) Chlamyrhodopsin represents a new type of sensory photoreceptor. *EMBO J.* **14**, 5849–5858.

Deininger, W., Fuhrmann, M. and Hegemann, P. (2000) Opsin evolution: out of wild green yonder? *Trends Genet.* **16**, 158–159.

Ding, D.Q., Chikashige, Y., Haraguchi, T. and Hiraoka, Y. (1998) Oscillatory nuclear movement in fission yeast meiotic prophase is driven by astral microtubules, as revealed by continuous observation of chromosomes and microtubules in living cells. *J. Cell Sci.* **111**(Pt 6), 701–712.

Drescher, K., Goldstein, R.E. and Tuval, I. (2010) Fidelity of adaptive phototaxis. *Proc. Natl Acad. Sci. USA*, **107**, 11171–11176.

Dutcher, S.K. and O'Toole, E.T. (2016) The basal bodies of *Chlamydomonas reinhardtii*. *Cilia*, **5**, 18.

Ebnet, E., Fischer, M., Deininger, W. and Hegemann, P. (1999) Volvoxrhodopsin, a light-regulated sensory photoreceptor of the spheroidal green alga *Volvox carteri*. *Plant Cell*, **11**, 1473–1484.

Edgar, R.C. (2004) MUSCLE: multiple sequence alignment with high accuracy and high throughput. *Nucleic Acids Res.* **32**, 1792–1797.

Ehler, L.L., Holmes, J.A. and Dutcher, S.K. (1995) Loss of spatial control of the mitotic spindle apparatus in a *Chlamydomonas reinhardtii* mutant strain lacking basal bodies. *Genetics*, **141**, 945–960.

Eisenberg, E. and Levanon, E.Y. (2003) Human housekeeping genes are compact. *Trends Genet.* **19**, 362–365.

Eisenberg, E. and Levanon, E.Y. (2013) Human housekeeping genes, revisited. *Trends Genet.* **29**, 569–574.

Felsenstein, J. (1989) Phylip – phylogeny inference package (Version 3.2). *Cladistics*, **5**, 164–166.

Foster, K.W., Saranak, J., Patel, N., Zarilli, G., Okabe, M., Kline, T. and Nakanishi, K. (1984) A rhodopsin is the functional photoreceptor for phototaxis in the unicellular eukaryote *Chlamydomonas*. *Nature*, **311**, 756–759.

Fuentealba, L.C., Eivers, E., Geissert, D., Taelman, V. and De Robertis, E.M. (2008) Asymmetric mitosis: Unequal segregation of proteins destined for degradation. *Proc. Natl Acad. Sci. USA*, **105**, 7732–7737.

Fuhrmann, M., Oertel, W. and Hegemann, P. (1999) A synthetic gene coding for the green fluorescent protein (GFP) is a versatile reporter in *Chlamydomonas reinhardtii*. *Plant J.* **19**, 353–361.

Fuhrmann, M., Stahlberg, A., Govorunova, E., Rank, S. and Hegemann, P. (2001) The abundant retinal protein of the *Chlamydomonas* eye is not the photoreceptor for phototaxis and photophobic responses. *J. Cell Sci.* **114**, 3857–3863.

Fuhrmann, M., Deininger, W., Kateriya, S. and Hegemann, P. (2003) Rhodopsin-related proteins, cop1, cop2 and chop1 in *Chlamydomonas reinhardtii*. In *Photoreceptors and Light Signalling. Comprehensive Series in Photochemical and Photobiological Sciences (series eds. G Jori and D-P Häder)*, (Batschauer, A. ed.). Cambridge, UK: The Royal Society of Chemistry, pp. 124–135.

Gao, S., Nagpal, J., Schneider, M.W., Kozjak-Pavlovic, V., Nagel, G. and Gottschalk, A. (2015) Optogenetic manipulation of cGMP in cells and animals by the tightly light-regulated guanylyl-cyclase opsin CyclOp. *Nat. Commun.* **6**, 8046.

Geimer, S. and Melkonian, M. (2004) The ultrastructure of the *Chlamydomonas reinhardtii* basal apparatus: identification of an early marker of radial asymmetry inherent in the basal body. *J. Cell Sci.* **117**, 2663–2674.

Geimer, S. and Melkonian, M. (2005) Centrin scaffold in *Chlamydomonas reinhardtii* revealed by immunoelectron microscopy. *Eukaryot. Cell*, **4**, 1253–1263.

Goldstein, R.E. (2015) Green algae as model organisms for biological fluid dynamics. *Annu. Rev. Fluid Mech.* **47**(47), 343–375.

Goodstein, D.M., Shu, S., Howson, R. *et al.* (2012) Phytozome: a comparative platform for green plant genomics. *Nucleic Acids Res.* **40**, D1178–1186.

Goold, H.D., Cuine, S., Legeret, B. *et al.* (2016) Saturating light induces sustained accumulation of oil in plastidal lipid droplets in *Chlamydomonas reinhardtii*. *Plant Physiol.* **171**, 2406–2417.

Gould, R.R. (1975) The basal bodies of *Chlamydomonas reinhardtii*. Formation from probasal bodies, isolation, and partial characterization. *J. Cell Biol.* **65**, 65–74.

Greiner, A., Kelterborn, S., Evers, H., Kreimer, G., Sizova, I. and Hegemann, P. (2017) Targeting of photoreceptor genes in *Chlamydomonas reinhardtii* via zinc-finger nucleases and CRISPR/Cas9. *Plant Cell*, **29**, 2498–2518.

Gruber, H., Kirzinger, S.H. and Schmitt, R. (1996) Expression of the *Volvox* gene encoding nitrate reductase: mutation-dependent activation of cryptic splice sites and intron-enhanced gene expression from a cDNA. *Plant Mol. Biol.* **31**, 1–12.

Hall, T.A. (1999) BioEdit: a user-friendly biological sequence alignment editor and analysis program for Windows 95/98/NT. *Nucleic Acids Symp. Ser.* **41**, 95–98.

Hallmann, A. (2003) Extracellular matrix and sex-inducing pheromone in *Volvox*. *Int. Rev. Cytol.* **227**, 131–182.

Hallmann, A. (2006) Morphogenesis in the family Volvocaceae: different tactics for turning an embryo right-side out. *Protist*, **157**, 445–461.

Hallmann, A. and Wodniok, S. (2006) Swapped green algal promoters: *aphVIII*-based gene constructs with *Chlamydomonas* flanking sequences work as dominant selectable markers in *Volvox* and vice versa. *Plant Cell Rep.* **25**, 582–591.

Hanschen, E.R., Marriage, T.N., Ferris, P.J. *et al.* (2016) The *Gonium pectorale* genome demonstrates co-option of cell cycle regulation during the evolution of multicellularity. *Nat. Commun.* **7**, 11370.

Harper, J.F., Huson, K.S. and Kirk, D.L. (1987) Use of repetitive sequences to identify DNA polymorphisms linked to *regA*, a developmentally important locus in *Volvox*. *Genes Dev.* **1**, 573–584.

Harris, E.H. (2001) *Chlamydomonas* as a model organism. *Annu. Rev. Plant Physiol. Plant Mol. Biol.* **52**, 363–406.

Harris, E.H., Stern, D.B. and Witman, G.B. (2009) *The Chlamydomonas Sourcebook*, 2nd edn. San Diego, CA: Academic Press.

Herron, M.D., Hackett, J.D., Aylward, F.O. and Michod, R.E. (2009) Triassic origin and early radiation of multicellular volvocine algae. *Proc. Natl Acad. Sci. USA*, **106**, 3254–3258.

Hofmann, K. and Stoffel, W. (1993) TMbase – a database of membrane spanning proteins segments. *Biol. Chem. Hoppe-Seyler*, **374**, 166.

Holmes, J.A. and Dutcher, S.K. (1989) Cellular asymmetry in *Chlamydomonas reinhardtii*. *J. Cell Sci.* **94**(Pt 2), 273–285.

Huskey, R.J., Semenkovich, C.F., Griffin, B.E., Cecil, P.O., Callahan, A.M., Chace, K.V. and Kirk, D.L. (1979) Mutants of *Volvox carteri* affecting nitrogen assimilation. *Mol. Gen. Genet.* **169**, 157–161.

Jones, D.T., Taylor, W.R. and Thornton, J.M. (1994) A model recognition approach to the prediction of all-helical membrane protein structure and topology. *Biochemistry*, **33**, 3038–3049.

Käll, L., Krogh, A. and Sonnhammer, E.L. (2004) A combined transmembrane topology and signal peptide prediction method. *J. Mol. Biol.* **338**, 1027–1036.

Käll, L., Krogh, A. and Sonnhammer, E.L. (2005) An HMM posterior decoder for sequence feature prediction that includes homology information. *Bioinformatics*, **21**(Suppl 1), i251–257.

Käll, L., Krogh, A. and Sonnhammer, E.L. (2007) Advantages of combined transmembrane topology and signal peptide prediction–the Phobius web server. *Nucleic Acids Res.* **35**, W429–432.

Kempeneers, C. and Chilvers, M.A. (2018) To beat, or not to beat, that is question! The spectrum of ciliopathies. *Pediatr. Pulmonol.* **53**, 1122–1129.

Kianianmomeni, A. (2015) Cell-type specific photoreceptors and light signaling pathways in the multicellular green alga *Volvox carteri* and their potential role in cellular differentiation. *Plant Signal. Behav.* **10**, e1010935.

Kianianmomeni, A. and Hallmann, A. (2014) Algal photoreceptors: in vivo functions and potential applications. *Planta*, **239**, 1–26.

Kianianmomeni, A. and Hallmann, A. (2015) Transcriptional analysis of *Volvox* photoreceptors suggests the existence of different cell-type specific light-signaling pathways. *Curr. Genet.* **61**, 3–18.

Kianianmomeni, A., Nematollahi, G. and Hallmann, A. (2008) A gender-specific retinoblastoma-related protein in *Volvox carteri* implies a role for the retinoblastoma protein family in sexual development. *Plant Cell*, **20**, 2399–2419.

Kirk, D.L. (1998) *Volvox: molecular-genetic origins of multicellularity and cellular differentiation*. Cambridge: Cambridge University Press.

Kirk, M.M. and Kirk, D.L. (1985) Translational regulation of protein synthesis, in response to light, at a critical stage of *Volvox* development. *Cell*, **41**, 419–428.

Kirk, D.L., Birchem, R. and King, N. (1986) The extracellular matrix of *Volvox*: a comparative study and proposed system of nomenclature. *J. Cell Sci.* **80**, 207–231.

Kirk, D.L., Kaufman, M.R., Keeling, R.M. and Stamer, K.A. (1991) Genetic and cytological control of the asymmetric divisions that pattern the *Volvox* embryo. *Dev. Suppl.* **1**, 67–82.

Klein, B., Wibberg, D. and Hallmann, A. (2017) Whole transcriptome RNA-Seq analysis reveals extensive cell type-specific compartmentalization in *Volvox carteri*. *BMC Biol.* **15**, 111.

Kreimer, G. (2009) The green algal eyespot apparatus: a primordial visual system and more? *Curr. Genet.* **55**, 19–43.

Kremers, G.J., Goedhart, J., van Munster, E.B. and Gadella, T.W. Jr (2006) Cyan and yellow super fluorescent proteins with improved brightness, protein folding, and FRET Förster radius. *Biochemistry*, **45**, 6570–6580.

Kröger, P. and Hegemann, P. (1994) Photophobic responses and phototaxis in *Chlamydomonas* are triggered by a single rhodopsin photoreceptor. *FEBS Lett.* **341**, 5–9.

Krogh, A., Larsson, B., von Heijne, G. and Sonnhammer, E.L. (2001) Predicting transmembrane protein topology with a hidden Markov model: application to complete genomes. *J. Mol. Biol.* **305**, 567–580.

Kumar, M., Thakur, V. and Raghava, G.P. (2008) COPid: composition based protein identification. *In Silico Biol.* **8**, 121–128.

Kyte, J. and Doolittle, R.F. (1982) A simple method for displaying the hydropathic character of a protein. *J. Mol. Biol.* **157**, 105–132.

Lauersen, K.J., Kruse, O. and Mussgnug, J.H. (2015) Targeted expression of nuclear transgenes in *Chlamydomonas reinhardtii* with a versatile, modular vector toolkit. *Appl. Microbiol. Biotechnol.* **99**, 3491–3503.

Lechtreck, K.F., Rostmann, J. and Grunow, A. (2002) Analysis of *Chlamydomonas* SF-assemblin by GFP tagging and expression of antisense constructs. *J. Cell Sci.* **115**, 1511–1522.

Lee, K., Choi, S., Yang, C., Wu, H.C. and Yu, J. (2013) Autofluorescence generation and elimination: a lesson from glutaraldehyde. *Chem. Commun.* **49**, 3028–3030.

Leliaert, F., Smith, D.R., Moreau, H., Herron, M.D., Verbruggen, H., Delwiche, C.F. and De Clerck, O. (2012) Phylogeny and molecular evolution of the green algae. *Crit. Rev. Plant Sci.* **31**, 1–46.

Lemieux, C., Vincent, A.T., Labarre, A., Otis, C. and Turmel, M. (2015) Chloroplast phylogenomic analysis of chlorophyte green algae identifies a novel lineage sister to the Sphaeropleales (Chlorophyceae). *BMC Evol. Biol.* **15**, 264.

Lerche, K. and Hallmann, A. (2009) Stable nuclear transformation of *Gonium pectorale*. *BMC Biotechnol.* **9**, 64.

Lerche, K. and Hallmann, A. (2013) Stable nuclear transformation of *Eudorina elegans*. *BMC Biotechnol.* **13**, 11.

Lerche, K. and Hallmann, A. (2014) Stable nuclear transformation of *Pandorina morum*. *BMC Biotechnol.* **14**, 65.

Letunic, I. and Bork, P. (2016) Interactive tree of life (iTOL) v3: an online tool for the display and annotation of phylogenetic and other trees. *Nucleic Acids Res.* **44**, W242–W245.

Loncarek, J. and Bettencourt-Dias, M. (2018) Building the right centriole for each cell type. *J. Cell Biol.* **217**, 823–835.

Long, H., Zhang, F., Xu, N., Liu, G., Diener, D.R., Rosenbaum, J.L. and Huang, K. (2016) Comparative analysis of ciliary membranes and ectosomes. *Curr. Biol.* **26**, 3327–3335.

Manuell, A.L. and Mayfield, S.P. (2006) A bright future for *Chlamydomonas*. *Genome Biol.* **7**, 327.

Markwardt, M.L., Kremers, G.J., Kraft, C.A., Ray, K., Cranfill, P.J., Wilson, K.A., Day, R.N., Wachter, R.M., Davidson, M.W. and Rizzo, M.A. (2011) An improved cerulean fluorescent protein with enhanced brightness and reduced reversible photoswitching. *PLoS ONE*, **6**, e17896.

Matasci, N., Hung, L.H., Yan, Z. *et al.* (2014) Data access for the 1,000 Plants (1KP) project. *Gigascience*, **3**, 17.

Matt, G. and Umen, J. (2016) *Volvox*: a simple algal model for embryogenesis, morphogenesis and cellular differentiation. *Dev. Biol.* **419**, 99–113.

Melkonian, M. (1978) Structure and significance of cruciate flagellar root systems in green algae: Comparative investigations in species of *Chlorosarcinopsis* (Chlorosarcinales). *Plant Syst. Evol.* **130**, 265–292.

Melkonian, M. and Robenek, H. (1980) Eyespot membranes of *Chlamydomonas reinhardii*: a freeze-fracture study. *J. Ultrastruct. Res.* **72**, 90–102.

Merchant, S.S., Prochnik, S.E., Vallon, O. *et al.* (2007) The *Chlamydomonas* genome reveals the evolution of key animal and plant functions. *Science*, **318**, 245–250.

Mittelmeier, T.M., Thompson, M.D., Lamb, M.R., Lin, H. and Dieckmann, C.L. (2015) MLT1 links cytoskeletal asymmetry to organelle placement in *Chlamydomonas*. *Cytoskeleton (Hoboken)*, **72**, 113–123.

Moestrup, Ø. (1978) On the phylogenetic validity of the flagellar apparatus in green algae and other chlorophyll A and B containing plants. *Biosystems*, **10**, 117–144.

Müller, T., Rahmann, S., Dandekar, T. and Wolf, M. (2004) Accurate and robust phylogeny estimation based on profile distances: a study of the Chlorophyceae (Chlorophyta). *BMC Evol. Biol.* **4**, 20.

Nagel, G., Ollig, D., Fuhrmann, M., Kateriya, S., Musti, A.M., Bamberg, E. and Hegemann, P. (2002) Channelrhodopsin-1: a light-gated proton channel in green algae. *Science*, **296**, 2395–2398.

Nagel, G., Szellas, T., Huhn, W., Kateriya, S., Adeishvili, N., Berthold, P., Ollig, D., Hegemann, P. and Bamberg, E. (2003) Channelrhodopsin-2, a directly light-gated cation-selective membrane channel. *Proc. Natl Acad. Sci. USA*, **100**, 13940–13945.

Natt, N.K., Kaur, H. and Raghava, G.P. (2004) Prediction of transmembrane regions of beta-barrel proteins using ANN- and SVM-based methods. *Proteins*, **56**, 11–18.

NCBI Resource Coordinators. (2018) Database resources of the National Center for Biotechnology Information. *Nucleic Acids Res.* **46**, D8–D13.

Nicholas, K.B., Nicholas, H.B. and Deerfield, D.W. (1997) GeneDoc: analysis and visualization of genetic variation. *EMBnet.news*, **4**, 14.

Niederreither, K. and Dolle, P. (2008) Retinoic acid in development: towards an integrated view. *Nat. Rev. Genet.* **9**, 541–553.

Nigg, E.A. and Stearns, T. (2011) The centrosome cycle: centriole biogenesis, duplication and inherent asymmetries. *Nat. Cell Biol.* **13**, 1154–1160.

Nigg, E.A., Cajanek, L. and Arquint, C. (2014) The centrosome duplication cycle in health and disease. *FEBS Lett.* **588**, 2366–2372.

Nugent, T. and Jones, D.T. (2009) Transmembrane protein topology prediction using support vector machines. *BMC Bioinformatics*, **10**, 159.

Okada, Y. and Hirokawa, N. (2000) Mechanism of the single-headed processivity: diffusional anchoring between the K-loop of kinesin and the C terminus of tubulin. *Proc. Natl Acad. Sci. USA*, **97**, 640–645.

Ozawa, S., Nield, J., Terao, A., Stauber, E.J., Hippler, M., Koike, H., Rochaix, J.D. and Takahashi, Y. (2009) Biochemical and structural studies of the large Ycf4-photosystem I assembly complex of the green alga *Chlamydomonas reinhardtii*. *Plant Cell*, **21**, 2424–2442.

Pasquier, C. and Hamodrakas, S.J. (1999) An hierarchical artificial neural network system for the classification of transmembrane proteins. *Protein Eng.* **12**, 631–634.

Prochnik, S.E., Umen, J., Nedelcu, A.M. *et al.* (2010) Genomic analysis of organismal complexity in the multicellular green alga *Volvox carteri*. *Science*, **329**, 223–226.

Pröschold, T., Marin, B., Schlösser, U.G. and Melkonian, M. (2001) Molecular phylogeny and taxonomic revision of *Chlamydomonas* (Chlorophyta). I. Emendation of *Chlamydomonas* Ehrenberg and *Chloromonas* Gobi, and description of *Oogamochlamys* gen. nov. and *Lobochlamys* gen. nov. *Protist*, **152**, 265–300.

Provasoli, L. and Pintner, I.J. (1959) Artificial media for fresh-water algae: problems and suggestions. In *The Ecology of Algae, a symposium held at the Pymatuning Laboratory of Field Biology on June 18 and 19, 1959* (Tryon, C.A. and Hartman, R.T., eds). Pittsburgh, PA: The Pymatuning Symposia in Ecology, Special Publication No. 2, University of Pittsburgh, pp. 84–96.

Rost, B., Casadio, R., Fariselli, P. and Sander, C. (1995) Transmembrane helices predicted at 95% accuracy. *Protein Sci.* **4**, 521–533.

Saitou, N. and Nei, M. (1987) The neighbor-joining method: a new method for reconstructing phylogenetic trees. *Mol. Biol. Evol.* **4**, 406–425.

Sasso, S., Stibor, H., Mittag, M. and Grossman, A.R. (2018) From molecular manipulation of domesticated *Chlamydomonas reinhardtii* to survival in nature. *eLife*, **7**, pii: e39233.

Schatten, H. and Sun, Q.Y. (2018) Functions and dysfunctions of the mammalian centrosome in health, disorders, disease, and aging. *Histochem. Cell Biol.* **150**, 303–325.

Schiedlmeier, B., Schmitt, R., Müller, W., Kirk, M.M., Gruber, H., Mages, W. and Kirk, D.L. (1994) Nuclear transformation of *Volvox carteri*. *Proc. Natl Acad. Sci. USA*, **91**, 5080–5084.

Schindelin, J., Arganda-Carreras, I., Frise, E. *et al.* (2012) Fiji: an open-source platform for biological-image analysis. *Nat Methods*, **9**, 676–682.

Schmidt, M., Gessner, G., Luff, M. *et al.* (2006) Proteomic analysis of the eyespot of *Chlamydomonas reinhardtii* provides novel insights into its components and tactic movements. *Plant Cell*, **18**, 1908–1930.

Schoppmeier, J., Mages, W. and Lechtreck, K.F. (2005) GFP as a tool for the analysis of proteins in the flagellar basal apparatus of *Chlamydomonas*. *Cell Motil. Cytoskeleton.* **61**, 189–200.

Shimozono, S., Iimura, T., Kitaguchi, T., Higashijima, S. and Miyawaki, A. (2013) Visualization of an endogenous retinoic acid gradient across embryonic development. *Nature*, **496**, 363–366.

Sineshchekov, O.A., Jung, K.H. and Spudich, J.L. (2002) Two rhodopsins mediate phototaxis to low- and high-intensity light in *Chlamydomonas reinhardtii*. *Proc. Natl Acad. Sci. USA*, **99**, 8689–8694.

Starr, R.C. (1969) Structure, reproduction and differentiation in *Volvox carteri* f. *nagariensis* Iyengar, strains HK 9 & 10. *Arch Protistenkd.* **111**, 204–222.

Starr, R.C. (1970) Control of differentiation in *Volvox*. *Dev. Biol. Suppl.* **4**, 59–100.

Starr, R.C. (1980) Colonial chlorophytes. In *Phytoflagellates* (Cox, E. R., ed). Amsterdam: Elsevier, pp. 147–163.

Starr, R.C. and Jaenicke, L. (1974) Purification and characterization of the hormone initiating sexual morphogenesis in *Volvox carteri* f. *nagariensis* Iyengar. *Proc. Natl Acad. Sci. USA*, **71**, 1050–1054.

Suzuki, T., Yamasaki, K., Fujita, S. *et al.* (2003) Archaeal-type rhodopsins in *Chlamydomonas*: model structure and intracellular localization. *Biochem. Biophys. Res. Commun.* **301**, 711–717.

Tian, Y., Gao, S., von der Heyde, E.L., Hallmann, A. and Nagel, G. (2018) Two-component cyclase opsins of green algae are ATP-dependent and light-inhibited guanylyl cyclases. *BMC Biol.* **16**, 144.

Tilbrook, K., Dubois, M., Crocco, C.D., Yin, R., Chappuis, R., Allorent, G., Schmid-Siegert, E., Goldschmidt-Clermont, M. and Ulm, R. (2016) UV-B perception and acclimation in *Chlamydomonas reinhardtii*. *Plant Cell*, **28**, 966–983.

Turmel, M., Gagnon, M.C., O'Kelly, C.J., Otis, C. and Lemieux, C. (2009) The chloroplast genomes of the green algae *Pyramimonas*, *Monomastix*, and *Pycnococcus* shed new light on the evolutionary history of prasinophytes and the origin of the secondary chloroplasts of euglenids. *Mol. Biol. Evol.* **26**, 631–648.

Ueki, N., Matsunaga, S., Inouye, I. and Hallmann, A. (2010) How 5000 independent rowers coordinate their strokes in order to row into the sunlight: phototaxis in the multicellular green alga *Volvox*. *BMC Biol.* **8**, 103.

Wagner, V., Ullmann, K., Mollwo, A., Kaminski, M., Mittag, M. and Kreimer, G. (2008) The phosphoproteome of a *Chlamydomonas reinhardtii* eyespot fraction includes key proteins of the light signaling pathway. *Plant Physiol.* **146**, 772–788.

Wang, L. and Dynlacht, B.D. (2018) The regulation of cilium assembly and disassembly in development and disease. *Development*, **145**, dev151407.

Wang, X., Tsai, J.W., Imai, J.H., Lian, W.N., Vallee, R.B. and Shi, S.H. (2009) Asymmetric centrosome inheritance maintains neural progenitors in the neocortex. *Nature*, **461**, 947–955.

Wood, C.R. and Rosenbaum, J.L. (2015) Ciliary ectosomes: transmissions from the cell's antenna. *Trends Cell Biol.* **25**, 276–285.

Wood, C.R., Huang, K., Diener, D.R. and Rosenbaum, J.L. (2013) The cilium secretes bioactive ectosomes. *Curr. Biol.* **23**, 906–911.

Zee, B.M. and Garcia, B.A. (2012) Discovery of lysine post-translational modifications through mass spectrometric detection. *Essays Biochem.* **52**, 147–163.

Zhou, Y., Yang, S., Mao, T. and Zhang, Z. (2015) MAPanalyzer: a novel online tool for analyzing microtubule-associated proteins. *Database*, **2015**, pii: bav108.